

Group 12 Dihalides: Structural Predilections from Gases to Solids

Kelling J. Donald,^{*,[a]} Magdolna Hargittai,^{*,[b]} and Roald Hoffmann^{*,[c]}

Abstract: Connections between the structures of Group 12 dihalides in their vapor and crystal phases are sought and discussed. The molecular structures of all monomers and dimers (MX_2 : $\text{M}=\text{Zn}, \text{Cd}, \text{Hg}$ and $\text{X}=\text{F}, \text{Cl}, \text{Br}, \text{I}$) were calculated at the density functional B3PW91 and MP2 computational levels. All the monomers are linear, with the mercury dihalide molecules having shorter bonds than their cadmium analogues; the ZnX_2 and CdX_2 structures are similar. The

shorter Hg–X distances are traced back to relativistic effects. For the dimers, many possible geometrical arrangements were considered. The zinc and cadmium dihalide dimers have the usual D_{2h} -symmetry geometry, whereas the mercury dihalide dimers are loosely-bound units with C_{2h} symmetry. The

Keywords: bonding • models • gas-phase structures • Group 12 elements • solid-state structures

origins of this C_{2h} structure are discussed from different points of view, including frontier orbital interactions. The crystals of Group 12 dihalides span a wide range of structure types, from three-dimensional extended solids to molecular crystals. There is an obvious connection between the structures and characteristics of monomers, their dimers, and the crystals they form. The similarities as well as startling differences from the Group 2 dihalides are analyzed.

Introduction

What happens to molecules at the borderline of ionic and covalent bonding as they pass from the vapor—where they are generally monomeric and dimeric—to the solid state? This question, which we have broached for the alkaline earth dihalides,^[1] is here pursued for the Group 12 dihalides, another class of molecules at an interface of bonding types.

The immense chemistry of the Group 12 metals Zn and Cd, less so Hg, is dominated by oxidation state 2.^[2] There-

fore, the bonding in Group 12 is generally regarded as similar to that of the main group alkaline earth elements. However, there are good theoretical reasons to believe that the chemistry of the elements of the two groups differ in many ways. First, there is an increase in the effective nuclear charge Z on the valence s electrons as the subvalent (d or f) atomic orbitals are filled going across the periodic table from Group 2 to Group 12.^[2,3] Second, there is the importance of relativistic effects for the heavier transition metals.^[3,4] And third, there is also an essential difference in the role of the nearby d orbitals; the $(n-1)d$ orbitals, empty in the Group 2 metals, are completely occupied in Group 12.

As the d orbitals in period 4 are filled going from Sc to Zn, the effective charge seen by the valence ($4s$ and $3d$) electrons increases, and thus there is an overall reduction in the atomic radii (the so-called “ d -block contraction”).^[5,6] This contraction phenomenon is apparent in period 5 (Y to Cd), as well, but is less pronounced in that row.^[7] In period 6, the filling of the first set of f atomic orbitals (the lanthanide $4f$ orbitals) has a similar effect on the radii of the transition metals, Au, and Hg. The increase in Z as the $4f$ orbitals are filled results in a significant contraction in the radius of these elements (the lanthanide contraction).^[3,6,8]

Relativistic effects, increasing roughly as Z^2 (see section 2; ref. [4]), become increasingly important as we go down the short group Zn to Hg.^[3,4,9] The influence of relativistic

[a] Prof. Dr. K. J. Donald
Department of Chemistry, Gottwald Center for the Sciences
University of Richmond, Richmond, Virginia 23173 (USA)
E-mail: kdonald@richmond.edu

[b] Prof. Dr. M. Hargittai
Materials Structure and Modeling Research Group of the Hungarian Academy of Sciences
Department of Inorganic and Analytical Chemistry
Budapest University of Technology and Economics
P.O. Box 91, 1521 Budapest (Hungary)
E-mail: hargittai@mail.bme.hu

[c] Prof. Dr. R. Hoffmann
Department of Chemistry and Chemical Biology
Cornell University, Ithaca NY, 14853 (USA)
E-mail: rh34@cornell.edu

Supporting information for this article is available on the WWW under <http://dx.doi.org/10.1002/chem.200801035>. See also ref. [82].

effects on the properties of the elements is already apparent in periods four and five (with a noticeable effect, for example, on the ionization energies of Cu, Zn, Ag, and Cd).^[3,8] But it is decisive for the chemistry of the sixth row transition elements, in particular for Au and Hg.^[3,4] Key to the present discussion, relativistic effects and the lanthanide contraction are cooperatively responsible for the electronegativity of Hg, χ_{Hg} , being larger than χ_{Zn} and χ_{Cd} .

Monomers: The significance of the differences in the shell structure and the physics of the atoms of Groups 2 and 12 for their chemistry is evident in the properties of their binary MX_2 dihalides, perhaps the best characterized molecules of the Group 12 metals.^[10–12] For the Group 2 dihalides, it is now well known that although all the BeX_2 and MgX_2 molecules are linear, some of the Ca, Sr, and Ba dihalides (CaF_2 , SrF_2 , SrCl_2 , and all the BaX_2 molecules) have a bent geometry.^[12–16] This initially surprising observation has been rationalized quite successfully by the involvement of $(n-1)d$ orbitals in the bonding and by the role of core-polarization interactions between the metal and halide sites.^[16] An explanation based on the pseudo-Jahn–Teller effect has also been given.^[17]

Nothing like this happens for Zn, Cd, and Hg, however; the dihalides of these elements are all linear.^[12,13b,c] This preference for a linear geometry in Group 12 dihalides has been explained by the unavailability of empty $(n-1)d$ orbitals (these are now filled) in the Group 12 metal atoms.^[18–20] There are empty nd orbitals, but they lie very high in energy. Figure 1 compares the averages of the relevant con-

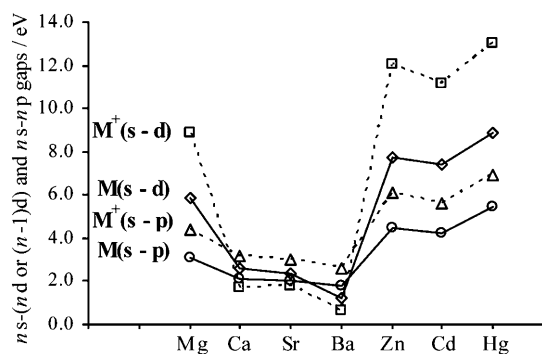


Figure 1. Average excitation energies for a valence ns electron of Groups 2 and 12 metal M atoms (solid line) and M^+ ions (dashed line) going to the np level and nearest empty d level: nd in Mg, $(n-1)d$ in Ca, Sr, and Ba and nd in Zn, Cd, and Hg (values obtained by averaging the $ns \rightarrow np$ and $ns \rightarrow (n-1, n)d$ separations compiled in ref. [21]).

figuration energies (see ref. [21]) for atoms of Groups 2 and 12. The severe limitations of purely electrostatic core polarization models,^[22,23,24] in particular, their failure to describe details of the bonding in the Group 12 dihalides, are discussed in reference [24].

Dimers: The significance of the relativistic and shell structure effects on the structural chemistry of the dihalides has

been identified in computational studies of the dihalide dimers as well.^[10–12,25] Unfortunately, there are no experimental geometries for the gas-phase dimers (M_2X_4) of the Group 12 dihalides. Could this be because the dimers are not thermodynamically stable? This is a point we will investigate in our work.

On the computational side, Kunciewicz-Kupczyk et al.^[26] have obtained a doubly bridged D_{2h} minimum-energy isomer (Figure 2a) for Cd_2I_4 , as did Kaupp and von Schne-

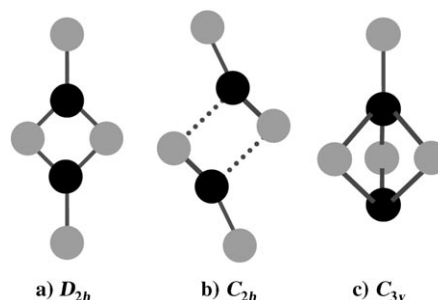


Figure 2. Minimum-energy structural isomers of the Group 12 (a) and (b) and Group 2 (a) and (c) dihalides.

ring^[11] for the Zn and Cd difluoride and dichloride dimers. The non-relativistic calculations performed by Kaupp and von Schnering predict D_{2h} minimum-energy isomers for Hg_2F_4 and Hg_2Cl_4 , as well, but when relativistic effects are included, the preferred structure is a loosely connected pair of monomers forming a doubly bridged structure of C_{2h} symmetry (see Figure 2b)!^[10,11,27] The C_{2h} structure may not seem too different from D_{2h} , but, as we will see, the metrics of the central ring betray a weak interaction of the monomers rather than simply an alternative symmetry choice for the dimer. This unique structural preference in the HgX_2 dimers for the C_{2h} structure has been linked by Kaupp and von Schnering to a relativistic reduction in charge separation in the $M-X$ bond going down the group from Zn to Hg.^[11] The triply bridged C_{3v} dimer structure (Figure 2c), strongly preferred by the bent Group 2 dihalides, was not considered by Kaupp and von Schnering, but that isomer is unlikely to be competitive for the Hg dihalides, given the weak bonding in the C_{2h} structure.^[10,11]

Extended structures: The extended solid structures of the Group 12 dihalides show significant diversity in their structure type preferences at ambient conditions. The twelve solids span the ionic three-dimensional extended (ZnX_2 , and the CdF_2 and HgF_2 fluorite), layered (CdCl_2 and CdI_2), and molecular (HgCl_2 , and HgBr_2) structure types.^[28] This is in significant contrast to the Group 2 dihalide extended solids, which at ambient conditions are mostly ionic layered and three-dimensional systems. The beryllium dihalides, except for BeF_2 ,^[29] form stacks of one-dimensional chains (the SiS_2 structure type). There are no known molecular solids for the Group 2 dihalides.

The work ahead: We begin with a brief discussion of the structural properties of the Group 12 dihalide monomers. An extensive survey of possible dimer geometries (including the three in Figure 2) follows. We are interested in both the geometry and the stability of the dimers, so the dimerization energies are also discussed in detail. We try out various simple frontier-orbital models to understand the weak bonding in HgX_2 dimers.

Next, we try to provide an assessment of how the structure types exhibited by the Group 12 dihalide solids may be understood based on clues picked up already from the geometric preferences and energetics of the isolated gas-phase structures. We want to find out the extent to which structural preferences in the Group 12 dihalide monomers or dimers carry over into or are “remembered” in the solids.

Theoretical methods: Optimized geometries of the monomer and dimer structures of the Group 12 dihalides have been obtained using the B3PW91^[30] density functional (DFT) method and the following basis sets: the correlation consistent polarized-valence triple-zeta (cc-pVTZ) all-electron basis set for F, Cl,^[31] the energy-consistent small-core MDF effective-core potentials (ECPs), leaving out the spin-orbit potential, but retaining the treatment of scalar-relativistic effects,^[32] and their associated cc-pVTZ basis sets (describing 25 valence electrons) for Br and I.^[33] For the metal sites, the MDF small core ECPs^[34] (without the spin-orbit part) were employed along with the corresponding cc-pVTZ bases for the 20 valence electrons of Zn, Cd, and Hg.^[35] So, for all large atoms, the orbitals of the $(n-1)$ shell were treated as part of the valence shell. To investigate the effect of relativity on structural preferences in the HgX_2 dimers, we performed non-relativistic structural optimizations as well for the mercury halides, using the MHF ECPs and basis sets at the Hg sites.^[36] The ECPs and basis sets described above for the halogen sites were used throughout.

All our theoretical calculations have been performed by using the Gaussian 03 suite of programs.^[37] Geometry optimizations for the most promising structures were repeated using the MP2 method. Frequency analyses were performed at the DFT level, using an ultrafine grid,^[38] and natural bond orbital (NBO) analyses were also carried out for all species.^[39]

To probe whether the different crystal structure types exhibited by each of the mercury dihalides could be stable for the other members of that series, we carried out a constrained energy minimization for each of the HgX_2 compounds in the various structure types using the projector augmented wave (PAW) method as implemented in the Vienna ab initio Simulation Package (VASP).^[40,41]

Results and Discussion

Structural preferences in the Group 12 dihalide monomers

Some 50 years ago, Akishin and Spiridonov applied the then fledgling gas-phase electron diffraction technique to

determine linear geometries for the Group 12 dihalides.^[42] Since then, the Group 12 dihalides have been studied extensively, with the more recent and more accurate electron diffraction experiments^[43–45] confirming linear geometries for all these molecules.

However, gas-phase electron diffraction cannot distinguish between linear and bent geometries if the molecules have large amplitude bending vibrations—which is the case here.^[12] Moreover, some of the earlier matrix isolation studies found nonlinear geometries for a number of the Group 12 dihalides, in particular for the HgX_2 structures.^[46] Incidentally, the determination in reference [46b] that some of the HgX_2 molecules are bent is a reversal from conclusions published a decade before^[47] in favor of linear geometries for all the molecules. In reference [46b], however, the authors did point out that the influence of the “inert” matrix was not taken into account. There is now ample evidence that interactions with the matrix can be decisive, causing significant changes in the vibrational spectra, leading, in turn, to apparently inaccurate geometry assignments (see, for example, ref. [48] and references therein). For binary dihalides, linear ground-state structures may appear to be bent, MgF_2 being a well known case.^[49]

The computational data do not show a similar ambiguity, however. Different levels, including various DFT, MP2, CCSD(T) and QCISD calculations, have consistently found linear minimum-energy structures for the Group 12 dihalide molecules.^[50–54]

Herein we present the first computational survey of the complete set of Group 12 dihalides since the initial local density functional (LDF) study of the monomers by Liao et al.^[53] In agreement with earlier studies, we have obtained linear geometries for all twelve molecules (see Table 1). Vibrational analyses yielded no imaginary frequency, indicating that a bent conformation is disfavored for all these compounds. The computed vibrational frequencies and force constants are listed in Table S1 in the Supporting Information. There is good agreement between the computed and

Table 1. Experimental and computed (B3PW91 and MP2) minimum-energy geometries of the Group 12 dihalide molecules.

Monomer	r [Å]			Shape ^[a]
	B3PW91	MP2	exptl ^[b]	
ZnF_2	1.722	1.707	1.727(6)	linear
ZnCl_2	2.073	2.051	2.064(5)	linear
ZnBr_2	2.212	2.182	2.194(9)	linear
ZnI_2	2.406	2.376	2.389(6)	linear
CdF_2	1.929	1.920		linear
CdCl_2	2.273	2.254	2.266(6)	linear
CdBr_2	2.405	2.381	2.386(5)	linear
CdI_2	2.590	2.568	2.570(6)	linear
HgF_2	1.923	1.897		linear
HgCl_2	2.267	2.229	2.240(7)	linear
HgBr_2	2.403	2.355	2.374(12)	linear
HgI_2	2.586	2.535	2.558(7)	linear

[a] See text for comments on disagreements in the historical experimental literature. [b] Experimental equilibrium bond lengths (also listed in ref. [12]) are estimated from measured thermal average values from refs. [43–45].

experimental bond lengths at both the DFT and the MP2 levels. The unsigned percentage deviation ($|r - r_{\text{expt}}| \times 100 / r_{\text{expt}}$) is quite small—between 0.25 % and 1.3 % (Table 1).

A remarkable feature of the MX_2 bond lengths listed in Table 1 is that the Hg–X distances are shorter than the Cd–X distances; based on the experimental bond lengths by about 0.01–0.03 Å. Although the differences in the corresponding calculated DFT distances are smaller, our higher-level MP2 calculations give differences of the same magnitude as the experimental ones (see Table S2 in the Supporting Information). This type of unexpected bond-length variation in molecules of transition metals down a column of the periodic table was attributed by Pyykkö to relativistic effects.^[3] The influence of relativity on the bond length is most evident in molecules of Groups 11 and 12 metals. Consider, for instance, the large difference between the experimental AuH and AgH bond lengths, with $r(\text{Au–H})$ being shorter by 0.094 Å than $r(\text{Ag–H})$.^[3] We have calculated the nonrelativistic bond lengths for the Group 12 dihalides (see Table S2 in the Supporting Information), and there the Hg–X bond lengths are longer than the Zn–X, and Cd–X bond lengths, as would be expected without taking relativistic effects into account. As also seen from Table S2, all the Group 12 dihalide bond lengths contract when relativistic effects are included. However, while the shortening is only about 0.02 to 0.04 Å for the ZnX_2 and CdX_2 molecules, it is more significant (≈ 0.12 Å) for the HgX_2 dihalides. *The relativistic contraction of the valence s orbital confers on Hg an atomic radius slightly smaller than that of Cd, hence the shorter Hg–X bond length for any X.*

Putting up resistance: the energy barrier to bending in the Group 12 dihalides: Dimerization and oligomerization will require bending. So, given that linear geometries are preferred for the Group 12 dihalides, how much would it cost in energy to bend these molecules? We approached this question by minimizing the molecular energy at fixed bond angles; the results for the fluorides and iodides are shown in Figure 3a,b (see Figure S1 in the Supporting Information for the data for all the halides).

The ZnX_2 and CdX_2 molecules show an almost identical resistance to bending (see Figure 3 and Figure S1 in the Supporting Information). In all four cases the relative energies of the Zn and Cd systems coincide until about $\theta = 145^\circ$. Thereafter, the lines become distinguishable, with the CdX_2 curves having the slightly smaller slope. Clearly, however, the mercury dihalides, having the steepest E versus θ curves in Figure 3 (see also Figure S1 in the Supporting Information), resist bending by a greater amount than do the Zn or Cd dihalides.

In assessing these differences in the relative energies, we might get some insight from what we know already about the Group 2 dihalides. It has been shown at various levels of theory that the rigidity of the Group 2 dihalide molecules, or, to be precise, the value of the bending force constant at $\theta = 180^\circ$, varies as $\text{BeX}_2 > \text{MgX}_2 > \text{CaX}_2 > \text{SrX}_2 > \text{BaX}_2$.^[1,14,15,20,23,24] This trend has been explained by the in-

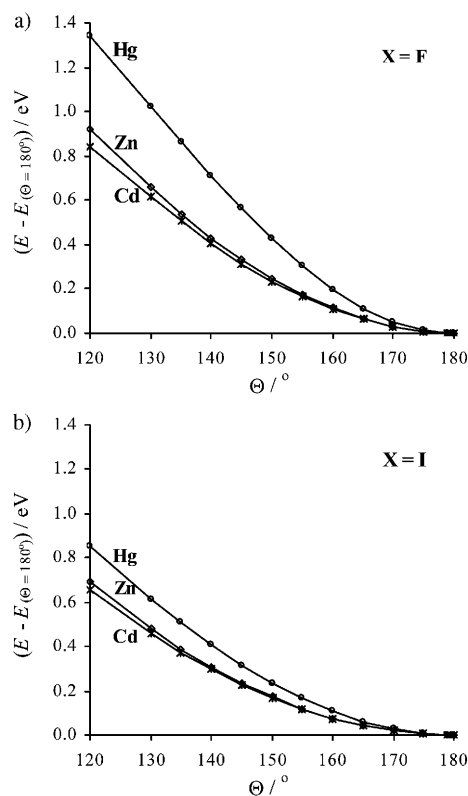


Figure 3. Computed bending potential energies for Group 12 difluorides (a) and diiodides (b).

creased polarizability or softness (or decreased electronegativity) of the metal center going from Be to Ba. For any halide X, the softer the metal center becomes, the more significantly it can be polarized by X and the greater the charge transfer along the M–X bond. These conditions promote and help to stabilize bent geometries in the metal dihalides. Simply put, the softer (more polarizable or less electronegative) the metal center is, the easier it is to bend the molecule.^[14,15,20,23,24]

Szentpály has computed identical values for the valence-state atomic softness σ of Zn and Cd ($\sigma = 0.338 \text{ eV}^{-1}$),^[14,20] and it is well known that the electronegativities of these two elements are similar (for Zn and Cd χ is 4.45 eV and 4.33 eV, respectively).^[55,56] Since these two atoms have similar softnesses/electronegativities, the ZnX_2 molecules and their CdX_2 analogues are expected to have a similar cost in energy for bending, consistent with the close resemblance in the energy profile shown in Figure 3.

The lanthanide contraction and relativistic effects combine to cause Hg to have an electronegativity value ($\chi_{\text{Hg}} = 4.91 \text{ eV}$) that is significantly larger than that of Zn and Cd (vide supra). So, for a given halide, X, $\Delta\chi_{\text{Hg–X}} = \chi_{\text{X}} - \chi_{\text{Hg}}$ will be smaller than $\Delta\chi_{\text{Zn–X}}$ and $\Delta\chi_{\text{Cd–X}}$. Since the charge shift $\delta_{\text{M–X}}$ varies directly with $\Delta\chi_{\text{M–X}}$, we anticipate that $\delta_{\text{Zn–X}} \approx \delta_{\text{Cd–X}} > \delta_{\text{Hg–X}}$. The bending is dependent on the M–X charge separation and the polarization of the metal center by the halides, so it is not surprising that the HgX_2 mole-

cules, for which we obtain the smallest δ values, show the least tendency to bend (have the largest slopes in Figure 3).

Charge distribution: The charge separation in the M–X bond (column 2 in Table 2) is quite similar for Zn and Cd for all X; the polarity of the bond decreases significantly

Table 2. NBO charge and orbital occupancy for the Group 12 dihalides from B3PW91 computations.

MX ₂	q_X/e	Orbital occupancy at M		
		<i>ns</i>	(<i>n</i> –1) <i>d</i>	<i>np</i>
ZnF ₂	–0.767	0.48	9.91	0.06
ZnCl ₂	–0.659	0.62	9.96	0.05
ZnBr ₂	–0.605	0.71	9.97	0.10
ZnI ₂	–0.533	0.81	9.98	0.13
CdF ₂	–0.747	0.54	9.90	0.06
CdCl ₂	–0.656	0.66	9.95	0.04
CdBr ₂	–0.605	0.74	9.96	0.08
CdI ₂	–0.541	0.84	9.97	0.10
HgF ₂	–0.656	0.88	9.75	0.04
HgCl ₂	–0.542	0.97	9.87	0.04
HgBr ₂	–0.493	1.03	9.90	0.04
HgI ₂	–0.433	1.10	9.93	0.10
Non-relativistic ^[a]				
HgF ₂	–0.763	0.49	9.92	0.06
HgCl ₂	–0.692	0.59	9.95	0.06
HgBr ₂	–0.647	0.66	9.96	0.08
HgI ₂	–0.588	0.75	9.97	0.10

[a] Non-relativistic calculations employing the MHF ECP and basis set for Hg.

going from F to I (from $q_F \approx -0.77e$ to $q_I \approx -0.53e$ for ZnX₂. Here and throughout this paper we are giving the charges in units of the absolute value of the electronic charge. Thus, $-0.77e$ means the fluorines are negatively charged). For the HgX₂ molecules, q_X also decreases going from F to I, but the charge separation ($q_F \approx -0.66e$ to $q_I \approx -0.43e$) is smaller than it is for the ZnX₂ and CdX₂ molecules.

Without relativistic effects (see Table S3 in the Supporting Information), the expected decrease in q_X as X gets larger is also observed. However, no significant reduction in q_X is observed in going from the ZnX₂ and CdX₂ systems to the HgX₂ molecules. The non-relativistic ZnX₂, CdX₂ and HgX₂ charge separations are, in fact, quite similar for each X (see Table S3 in the Supporting Information).

The relativistic reduction in the charge shift (reduced ionicity) going from Zn and Cd to Hg has been identified previously by Kaupp and von Schering for the difluorides and dichlorides.^[11] They also pointed out a corresponding decrease in the atomization energy of the HgX₂ molecules, noting that both of these observations are consistent with a significant relativistic stabilization of the occupied Hg valence s orbital and the corresponding increase in the Hg ionization energy.^[10,11]

Notice that although the charge separation in the molecules is reduced by relativistic effects, the bond lengths are shorter for the relativistic geometries (see Table 1 and Table S2 in the Supporting Information). The contraction of the valence s orbital makes charge transfer from that orbital

more difficult, and requires that the M and X atoms come closer to each other for bonding—hence the shorter and less polar (more covalent) bonds.

Valence *np* orbital (non-)involvement: What would a simple MO picture of bonding in MX₂ halides suggest? Figure 4 is a schematic interaction diagram: the *ns* and *np* orbitals of

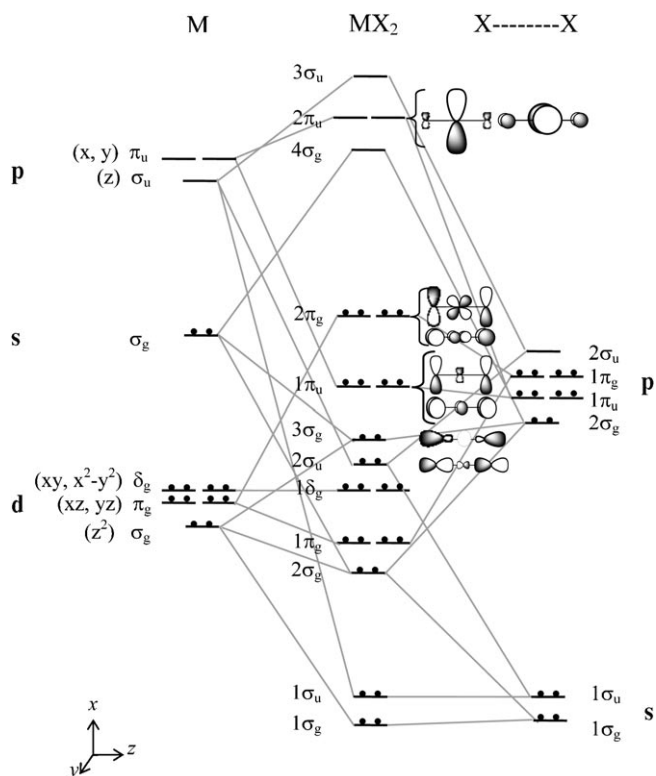


Figure 4. Schematic interaction diagram for a linear MX₂ molecule, built from a Group 12 metal atom M and an X₂ fragment.

two non-interacting halogens are at right, the filled (*n*–1)*d*, *ns* and the empty *np* orbitals of the metal are at left. Somewhat arbitrarily, the M *ns* level is placed at about the same energy as the X *np* orbitals. Of the resulting valence MOs, all but four in the scheme are filled. The orbital shapes in Figure 4 correspond roughly to the orbital contributions obtained in our DFT calculations.

The highest occupied MOs ($2\pi_g$, $1\pi_u$) are mainly halogen p combinations with a small bonding admixture of metal d and p orbitals. More important to the common picture of the M–X bond in MX₂ are the orbitals directly below, $3\sigma_g$ and $2\sigma_u$. The delocalized equivalent of two localized M–X bonds (Figure 5, left) are the σ_g and σ_u MOs at right. These

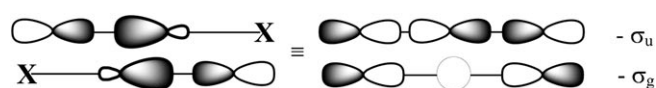


Figure 5. Simple representation of two localized MX₂ σ bonds and equivalent delocalized MOs.

are best approximated in a delocalized picture by $3\sigma_g$ and $2\sigma_u$.

The actual DFT orbitals (see Figure 6) show a noticeable metal s contribution in $3\sigma_g$, but almost no metal p contribution in $2\sigma_u$; the orbital occupations summed over all occu-

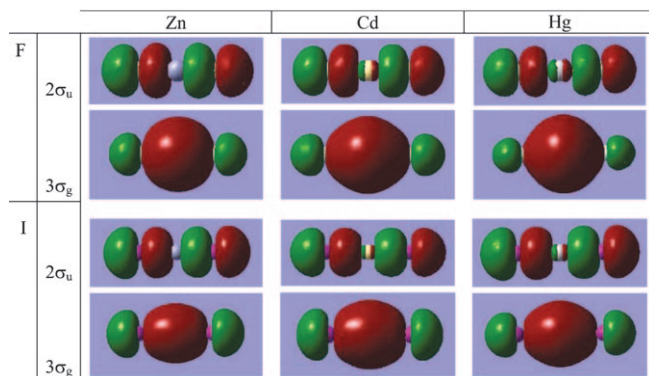


Figure 6. Picture of the $2\sigma_u$ and $3\sigma_g$ MOs from the DFT (B3PW91) calculations, constructed using the Gaussview program with an isovalue of 0.02 and a medium cube grid. (Note that the MOs are rendered in red and green. Small colored balls along the axis of the structures denote the different atoms: Zn, Cd, Hg, F, and I).

ried MOs in Table 2 are in accord with this. Pictures of all 17 MX_2 MOs are provided in Figure S2 in the Supporting Information for HgF_2 .

A lesser admixture of the metal (compared to halogen) orbital contribution in these MOs would be expected on electronegativity grounds. What is surprising, nonetheless, is the minimal participation of the M p orbitals in bonding. The σ_u orbital is nearly a lone-pair combination of the X ligands. Importantly, the poor participation of the p orbitals in the M–X bond is essentially independent of relativistic effects; the p orbital occupancies we have obtained for the non-relativistic calculations (Table 2 and Table S3 in the Supporting Information) are very similar to the relativistic values in Table 2 (see also refs. [10], and [11]).

The percentage contribution of the metal M (*ns*, *np*, and $(n-1)d$) atomic orbitals to the M–X bond orbitals in the Group 12 dihalides are plotted in Figure 7. Consistent with the low occupancy of that orbital (Table 2), we observe very little involvement of the *np* orbital in the bond. The $(n-1)d$ orbital contribution becomes more significant for the Hg dihalides (we comment on this observation in the next section), but the *p* orbital involvement is always poor; and is least for the Hg dihalides (see also Table S4 in the Supporting Information).

Might the energy separation between the M *ns* and *np* orbitals provide a way into understanding the small p participation in the bonding? In Figure 1, the s–p gap is significant (compared to the Group 2 atoms and M^+ ions), even for Zn and Cd where relativistic effects are less important than they are in Hg. The gap in Hg is evidently enlarged by the relativistic contraction of the s orbital, hence the discontinuities at Cd in Figure 1. The Hg atom has the largest s–p sep-

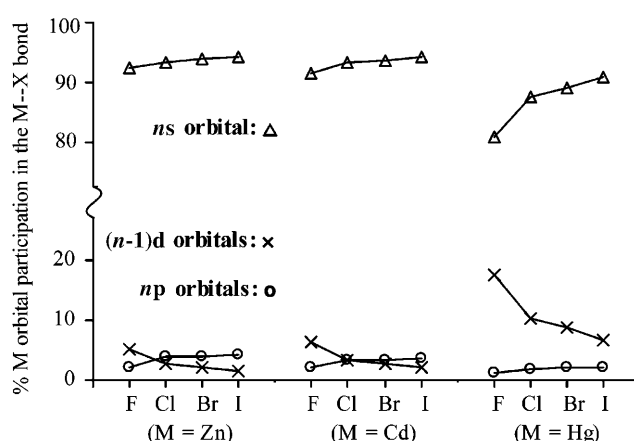


Figure 7. Percentage s, p, and d character of the metal hybrid orbital involved in the M–X bond of the Group 12 dihalide, MX_2 , molecules.

aration, although there is a decrease in the gap from Zn to Cd. The relatively high energy of the M p orbitals mitigates against their involvement in bonding. In a way, these MX_2 systems are close to a classical three-center electron-rich bonding situation (as in $F-H-F^-$, say), in which the central atom bonds only or predominantly through its s orbital.

Valence $(n-1)d$ orbital (non-)involvement: The $(n-1)d$ orbitals of Zn and Cd are hardly involved in the bonding in the ZnX_2 and CdX_2 molecules (see Figure 7 and Table S4 in the Supporting Information). The NBO $(n-1)d$ orbital contributions to the metal bonding in ZnF_2 and CdF_2 are only 5.3% and 6.4% respectively (see Table S4 in the Supporting Information). As X gets less electronegative, the d orbital participation falls off rapidly; for ZnI_2 and CdI_2 the contributions decrease to 1.6% and 2.2%, respectively.

The d orbital participation is more significant in the HgX_2 molecules. For example, the contribution of the $(n-1)d$ orbital to the Hg bonding is about 18% in HgF_2 and 7% in HgI_2 . Note that the increased d orbital participation on going from Zn and Cd to Hg is accompanied by a decrease in both the s and the already very poor p orbital contributions (see Figure 7 and Table S4 in the Supporting Information). The increased involvement of the d orbitals in the Hg bonding is evident in the orbital occupancy data (see Table 2). There is almost no electron transfer from the $(n-1)d$ orbital in the ZnX_2 and CdX_2 molecules, with the Zn and Cd $(n-1)d$ orbital occupancies always higher than 99% (occupancies ≥ 9.9 electrons). For the HgX_2 molecules the contribution of the $(n-1)d$ orbital to the bonding is a bit more significant; that is, the orbital occupancies are slightly smaller: 97.5% in HgF_2 , and increasing to 99.3% in HgI_2 . This increased involvement of the $(n-1)d$ orbitals is explained by the secondary destabilization of the $(n-1)d$ atomic orbital, which accompanies the relativistic stabilization of *ns* orbitals.^[57]

Of the three Group 12 metals, only the Hg $(n-1)d$ orbitals shows an important *valence-like* behavior in the HgX_2 molecules. For the more electronegative halides, in particu-

lar, the set of occupied 5d orbitals of Hg plays a key role in the bonding. As mentioned previously, the d orbital participation at the metal in HgF_2 is about 18%. The significant role of the 5d orbitals in the bonding of Hg (in clusters and in the bulk) has already been identified by Singh,^[58] who concluded that the 5d electrons must be treated as valence electrons to get reliable descriptions of the electronic structures of Hg clusters and solids. Our observations provide more evidence that this is true for Hg in molecules, as well.

Group 12 dihalide dimers

Dimers have been identified in small amounts in the vapors of the Group 12 dihalides by various experimental studies spanning at least the last forty years (see ref. [26,47,59,60]) and references therein). However, there are no available experimental geometrical parameters for them because of their minute concentrations in the vapor. According to mass spectrometric studies of ZnI_2 ^[60] and CdI_2 ^[26] vapors, the concentration of the dimers was roughly three orders of magnitude smaller than the monomer concentration. By 1969, the D_{2h} geometry (Figure 2a) was postulated for all the dimers, based on spectroscopic evidence.^[47] Nevertheless, geometrical parameters remain elusive for these systems.

Computational data are relatively sparse for the Group 12 dihalide dimers. Kaupp et al. carried out an extensive study of the dimers (covering all the Hg_2X_4 structures,^[10] and the zinc and cadmium difluoride and dichloride dimers^[11]), focusing on the influence of relativistic effects on their geometries. The only other computational study was that of the CdI_2 dimer by Kunciewicz-Kupczyk et al.^[26] The full series (M_2X_4 , $\text{M} = \text{Zn}, \text{Cd}$ and Hg and $\text{X} = \text{F}, \text{Cl}, \text{Br}$, and I) has not been examined so far in any study, as far as we know, not even at relatively low computational levels. In the present article, we study all twelve dimers, and examine an exhaustive set of possible isomer geometries.

Structural preferences: Eleven possible dimer geometries, shown in Figure 8, including the D_{2h} , C_{2h} , and C_{3v} isomers in Figure 2, have been examined. These are chosen for a variety of reasons: they are real or candidate structures for Group 2 dimers, they represent logical outcomes of frontier

orbital considerations, or just because of their symmetries are observed elsewhere in the periodic table.

To determine the most stable geometry for each of the dimers, the isomer structures (Figure 8) were optimized beginning with reasonable starting points in each case. The computed energies for the optimized isomers ii to xi relative to the energy of the doubly-bridged D_{2h} structure (isomer i in Figure 8), are listed in Table S5 in the Supporting Information. The corresponding numbers of imaginary frequencies obtained for all the optimized structures are listed in Table S6 in the Supporting Information.

The three most competitive geometries (D_{2h} , $C_{2h}(1)$, and C_{3v}) will be discussed in detail. Of the remaining eight structures, potential isomers vii–x are unstable relative to the D_{2h} structure. Each of those structures collapses to an effective D_{2h} structure; with the terminal halide only slightly misaligned ($<1^\circ$) relative to the terminal halides in the ideal D_{2h} structure. Isomer vi, a C_{2v} structure with one bent monomer coordinated to another bent monomer perpendicular to it, is also unstable, and flies apart in all 12 cases. The same “explosive” behavior is observed in most cases for isomer v as well. For that structure (with one linear monomer bonded end-on to the metal center of a bent monomer), the three M_2F_4 and the Cd_2Cl_4 dimers do not break apart (see Table S7 in the Supporting Information), but none is a local minimum on the M_2X_4 potential-energy surface (see Table S6 in the Supporting Information).^[61] The quadruply bridged D_{4h} isomer iv, splendid in its symmetry, is always much higher in energy than the D_{2h} structure. It is only a transition structure for the fluorides and Cd_2Cl_4 , and a third order saddle point in all the other cases (see Table S6 in the Supporting Information). Investigation of the D_{2d} geometry (xi, with X–M–X variable) was motivated by the great body of work showing direct attractive interactions between Au^{I} centers, the so-called aurophilic interaction. In the Zn^{II} , Cd^{II} , Hg^{II} halide cases we studied, the structures “exploded” to give two linear monomers each time.

The three remaining structures in Figure 8 are: i) D_{2h} , ii) $C_{2h}(1)$, and iii) C_{3v} ; their relative energies and the number of their imaginary frequencies are given in Table 3. The triply bridged C_{3v} isomers are always higher in energy than the D_{2h} structure (by 0.70–1.60 eV). They are local minima on the potential energy surfaces of all the Cd_2X_4 and Zn_2X_4

structures, except for Zn_2Cl_4 , for which we obtained two imaginary frequencies.^[62] For Zn_2Br_4 and Zn_2I_4 , the corresponding frequencies are positive, but very small ($\nu = 5.3 \text{ cm}^{-1}$ and 3.9 cm^{-1} , respectively) and are likely to be very sensitive to basis set and ECP choice; see footnote to Table 3). The Hg_2X_4 C_{3v} structures, all four of them, have two imaginary frequencies.^[62,63] The geometrical parameters of

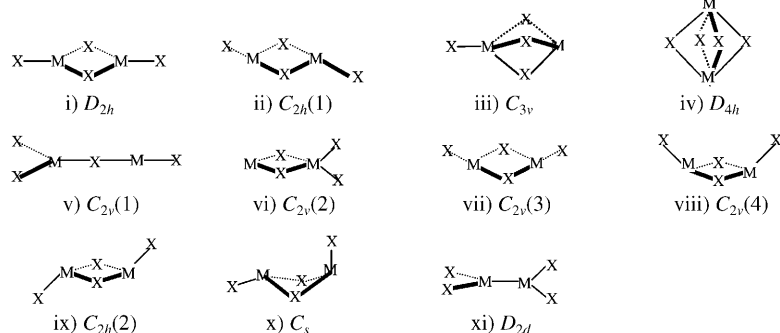


Figure 8. Possible dimer structures.

Table 3. Relative energies ($\Delta E = E(\text{isomer}) - E(D_{2h})$) [eV] of possible isomers or the Group 12 dihalide dimers, and the number of imaginary vibrational frequencies, n , obtained for the D_{2h} , C_{2h} , and C_{3v} isomers of the Group 12 dihalide dimers.^[a]

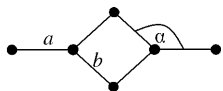
Dimer	ΔE [eV]		n	C_{2h} (1)	C_{3v} [b]
	C_{2h} (1)	C_{3v}			
Zn_2F_4	D_{2h}	1.17	0	D_{2h}	0
Zn_2Cl_4	D_{2h}	1.00	0	D_{2h}	2
Zn_2Br_4	D_{2h}	0.88	0	D_{2h}	0
Zn_2I_4	D_{2h}	0.76	0	D_{2h}	0
Cd_2F_4	D_{2h}	0.97	0	D_{2h}	0
Cd_2Cl_4	D_{2h}	0.90	0	D_{2h}	0
Cd_2Br_4	D_{2h}	0.81	0	D_{2h}	0
Cd_2I_4	D_{2h}	0.73	0	D_{2h}	0
Hg_2F_4	-0.53	1.55	1	0	2
Hg_2Cl_4	-0.46	1.30	1	0	2
Hg_2Br_4	-0.33	1.13	1	0	2
Hg_2I_4	-0.20	0.99	1	0	2

[a] The relative energies and the number of imaginary vibrational frequencies (always $n=0$) for the preferred structures are in bold type. [b] The different behavior of the Zn_2Cl_4 molecule might be coincidental; for possible explanations see ref. [63]. It may be that the vibrational frequencies are imaginary, or very small but real, for the three heavier Zn_2X_4 ($\text{X} = \text{Cl}, \text{Br}, \text{and I}$). For the C_{3v} Zn_2F_4 the vibrational frequency for the said degenerate vibrations is much larger, $\nu = 66 \text{ cm}^{-1}$, suggesting that the C_{3v} structure is probably a true minimum on this potential energy surface. The imaginary frequencies obtained for the two degenerate vibrations in the Hg_2X_4 molecules are rather large ($\nu = -84, -71, -53$, and -44 cm^{-1} for $\text{X} = \text{F}, \text{Cl}, \text{Br}, \text{and I}$ respectively), so, the C_{3v} structures are well established second-order saddle points on the Hg_2X_4 potential energy surfaces.

all the C_{3v} dimer structures are given in Table S8 in the Supporting Information.

The D_{2h} isomer is the minimum energy structure for all the ZnX_2 and the CdX_2 dimers. In fact, all eight of the ZnX_2 and CdX_2 C_{2h} (1) structures (isomer ii in Figure 8) collapse readily to the higher symmetry D_{2h} structure, whose geometrical parameters are given in Table 4. The computed vibrational frequencies for all the D_{2h} dimers are given in Table S9 in the Supporting Information.

Table 4. Optimized geometries of the D_{2h} dimer structures.^[a]

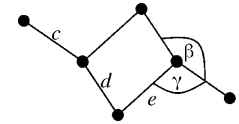


D_{2h}	a	b	α
Zn_2F_4	1.742	1.924	139.3
Zn_2Cl_4	2.100	2.291	133.1
Zn_2Br_4	2.241	2.430	131.6
Zn_2I_4	2.437	2.624	130.3
Cd_2F_4	1.951	2.138	141.9
Cd_2Cl_4	2.297	2.504	135.6
Cd_2Br_4	2.432	2.634	133.7
Cd_2I_4	2.618	2.817	131.9
Hg_2F_4	1.952	2.178	144.2
Hg_2Cl_4	2.297	2.535	137.6
Hg_2Br_4	2.432	2.664	135.8
Hg_2I_4	2.617	2.837	133.8

[a] The geometries are in italics where the D_{2h} isomer is not a minimum on the potential energy surface.

The HgX_2 dimers are different: The D_{2h} isomer is only a transition structure on the potential energy surface ($n=1$ in Table 3) for all four molecules. Instead, the minimum-energy arrangement for the HgX_2 dimers is the C_{2h} (1) geometry, see Table 5. These structures may be described as a sig-

Table 5. Optimized geometries of the HgX_2 C_{2h} (1) dimers.^[a]



C_{2h} (1)	c	d	e	β	γ
HgF_2	1.923	1.958	2.680	177.0	110.2
HgCl_2	2.267	2.291	3.290	175.9	99.9
HgBr_2	2.405	2.428	3.410	174.8	97.9
HgI_2	2.591	2.610	3.655	173.7	96.7

[a] The C_{2h} (1) ZnX_2 and CdX_2 isomers symmetrize to D_{2h} structure.

nificant distortion of the D_{2h} isomers, involving an increase in the bond angle α (cf. α in Table 4 and β in Table 5) and having very different bridging bonds (compare b in Table 4 with d and e in Table 5). Bonds d are about the same as the monomer bond, while bonds e in the C_{2h} (1) dimers are much longer (by some 0.76 \AA for Hg_2F_4 , and 1.07 \AA for Hg_2I_4) than the corresponding Hg-X bonds in the monomer (see Table 1). Such long bridging contacts are not observed in the D_{2h} ZnX_2 or CdX_2 dimers, where the bridging M-X distances are never more than 0.23 \AA longer than the M-X distances in the corresponding monomer (see Table 1).

It is obvious that the C_{2h} dimers (see Table 5) are but weakly interacting HgX_2 monomers—notice that $c \cong d$, and β is just a little bit down from 180° . The separation in energy between the C_{2h} (1) and D_{2h} isomers of Hg_2X_4 is rather small, only 0.20 eV for the iodides (Table 3, column 2), increasing by $\approx 0.11 \text{ eV}$ as X gets smaller going up the group from I to F. The vibrational frequencies of the minimum energy C_{2h} Hg_2X_4 isomers are given in Table S10 in the Supporting Information. The geometries of the most stable isomers (the Zn_2X_4 and Cd_2X_4 D_{2h} and Hg_2X_4 C_{2h} structures) were also obtained at the MP2 level, using the same relativistic ECPs and basis sets. The geometrical parameters are listed in Tables S11 and S12 in the Supporting Information—apart from actual metrical differences, they paint the same picture as the DFT results.

Preference for the D_{2h} structures in the ZnX_2 and CdX_2 dimers is in agreement with previous computational studies on some of the Group 12 dihalides.^[11,26] The fact that the linear ZnX_2 and CdX_2 molecules form D_{2h} -symmetry dimers is also consistent with an observed link between the structural preferences in the Group 2 dihalide monomers and the dimers they form. We have found computationally in refs. [1] and [64] that, among the Group 2 binary dihalides, the rigid linear monomers (e.g., BeX_2 and MgX_2) strongly prefer the D_{2h} dimer geometry, while the monomers that are bent (e.g. BaF_2 and SrF_2) show a strong preference for the C_{3v} geometry. For the linear Group 2 dihalide monomers,

the cost in energy to prepare (stretch and bend) the monomer fragments with the much smaller bond angles of the C_{3v} isomer or other higher-order bridged structures (such as the D_{4h} possibility; see Figure 8) are too expensive to be counterbalanced by the stabilization upon dimerization.^[1]

The $C_{2h}(1)$ structure preferred by HgX_2 dimers is exceptional, and we will discuss it presently. The mercury dihalides are apparently too rigid, and the stabilization via dimer formation too small, for even the D_{2h} structure to be stabilized significantly; not to speak of the C_{3v} geometry. Hence, a dimer structure ($C_{2h}(1)$) requiring minimal bending in the monomer fragments is preferred. Kaupp and von Schnering found previously that relativistic effects were decisive in stabilizing the $C_{2h}(1)$ geometry of the HgX_2 dimers compared to the D_{2h} structure.^[10] To investigate this inference, the D_{2h} and $C_{2h}(1)$ geometries of the HgX_2 dimer structures were recomputed at the B3PW91 level, employing the non-relativistic Hg MHF ECP and the corresponding 20-valence-electron basis set at the Hg sites. For the halides, the ECPs and basis sets described in the Methods Section above were used. Confirming the earlier results, we find that at the non-relativistic level all the D_{2h} Hg_2X_4 isomers (see geometries summarized in Table S13 in the Supporting Information) appear to be true minima and, in fact, the starting $C_{2h}(1)$ Hg_2X_4 structures optimize to effective D_{2h} geometries. It is evident, therefore, that relativistic effects in the mercury atom play a significant role in determining the structures of the HgX_2 dimers. In the next sections we investigate the reasons for these structural preferences in the Group 12 dimers.

Deformation energies: The cost in energy to deform the optimized monomer structures to the shapes they have in the D_{2h} and the $C_{2h}(1)$ dimers (the deformation energy, E_{def}) has been calculated by subtracting the computed energy of the linear monomers from the energy of the distorted monomer fragments as they appear in the dimers (see footnote a to Table 6). The more rigid the linear molecule is, the larger the deformation energy will be. Molecules that are very flexible or floppy have a low barrier to bending (and stretching), and will have relatively small deformation energies.

As expected from looking at the dimer geometries, the deformation energies for the monomer fragments in the $C_{2h}(1)$ HgX_2 dimers are rather insignificant compared to those for the D_{2h} structures (see Table 6). The reason is clear - the bond lengths (r) and the bond angle ($\theta = 180$) in the

monomers (see Table 1) are modified only slightly in preparing the $C_{2h}(1)$ monomer fragments (cf. c , d and β in Table 5).

The deformation energies we have obtained for the D_{2h} isomers are pretty large (see Table 6). They are, in fact, comparable to the corresponding values obtained in ref. [1] for the most rigid linear molecules (BeX_2 and MgX_2), and are much larger than the values obtained for the linear dihalides of Ca or Sr.^[1] The deformation energies for the C_{3v} isomers (not presented) are still larger (between 3.0 eV and 4.5 eV for the Zn, Cd and Hg difluorides). We can understand why the C_{3v} geometry does not stand much of a chance for the Group 12 dihalides.

Notice that, although the extent of the bending in the MX_2 fragments of the M_2X_4 D_{2h} dimers increases (i.e., α decreases) going from the fluoride to the iodide, for all M (see Table 4), the cost to bend the fragments, E_{def} , decreases in the same direction. This observation is consonant with the trends in Figure 3 for $X = F$ and I (and in Figure S1 in the Supporting Information for all X). Going from F to I, for any M, the energy needed to bend the monomer decreases significantly. A similar variation in the ease of bending as a function of X is observed for the linear Group 2 (Be and Mg) dihalides.^[1,65]

Another key feature of the deformation energy data is the large values we obtain for the D_{2h} HgX_2 dimers. The E_{def} values decrease from the ZnX_2 to the CdX_2 dimers, which is the kind of variation observed in the Group 2 dihalides, as well, going down that group.^[1] Going from the Cd to the Hg systems, however, the deformation energy increases considerably. This large cost in energy to prepare the HgX_2 D_{2h} dimers (large E_{def} in Table 6) is remarkable since the monomer fragments in these structures are less bent (have larger

Table 6. Computed (B3PW91) energies for the rearrangement of pairs of stable MX_2 monomers to the shapes observed in the two most stable M_2X_4 dimers, $E_{def}^{[a]}$, the counterpoise corrected dimerization Energies, $E_{dim}^{[b,c]}$, and enthalpies, $H_{dim}^{[d]}$.

Preferred isomer		E_{def} [eV]		E_{dim} [eV]		H_{dim}	
		$E_{def}(D_{2h})$	$E_{def}(C_{2h})$	$E_{dim}(D_{2h})$	$E_{dim}(C_{2h})$	calcd ^[d]	exptl.
Zn_2F_4	D_{2h}	1.53		-1.06 [-1.14] ^[e]			
Zn_2Cl_4	D_{2h}	1.47		-0.64 [-0.52] ^[e]			
Zn_2Br_4	D_{2h}	1.37		-0.62			
Zn_2I_4	D_{2h}	1.25		-0.57		-0.56 [-0.52]	-0.93(4) ^[g]
Cd_2F_4	D_{2h}	1.27		-1.11 [-1.34] ^[e]			
Cd_2Cl_4	D_{2h}	1.26		-0.66 [-0.63] ^[e]			
Cd_2Br_4	D_{2h}	1.21		-0.62			
Cd_2I_4	D_{2h}	1.12		-0.57		-0.55 [-0.58]	-0.71(7) ^[h]
Hg_2F_4	C_{2h}	1.97	0.04	0.31	-0.28 [-0.62] ^[f]		
Hg_2Cl_4	C_{2h}	1.76	0.01	0.38	-0.09 [-0.24] ^[f]		
Hg_2Br_4	C_{2h}	1.60	0.03	0.27	-0.06 [-0.22] ^[f]		
Hg_2I_4	C_{2h}	1.43	0.03	0.17	-0.03 [-0.24] ^[f]		

[a] $E_{def}(D_{2h}) = 2[E(X^dM^bX) - E(X^cM^cX)]$. Similarly, $E_{def}(C_{2h}(1)) = 2[E(X^cM^dX) - E(X^cM^cX)]$ (see Tables 4 and 5). [b] $E_{dim} = (E^{CP}(M_2X_4) \times 2 \times E(MX_2))$. The correction for basis set superposition errors has been accomplished by the addition of a counterpoise correction to the computed energy, so $E^{CP}(M_2X_4) = E(M_2X_4) + \delta^{CP}$. The counterpoise correction, δ^{CP} , and $E(M_2X_4)$ were obtained at the same computational level (see the Methods Section). [c] The values of E_{def} and E_{dim} for the preferred structures are in bold type. [d] $H_{dim} = (H^{CP}(M_2X_4) - 2 \times H(MX_2))$. DFT (B3PW91) and MP2 [in brackets] computed dimerization enthalpies, obtained from the difference between the MX_2 molecular enthalpies corrected for zero point energies (ZPEs) and thermal corrections at 298 K and the corresponding enthalpies for the dimers are given only where experimental data are available for comparison. [e] See ref. [11]. [f] See ref. [10]. [g] From mass spectrometry, see ref. [60]. [h] From mass spectrometry, see ref. [26].

α values) than the corresponding MX_2 fragments in the Zn_2X_4 and Cd_2X_4 molecules for any X (see α values in Table 4). Clearly, as was observed already in Figure 3, the HgX_2 monomers are more rigid than the ZnX_2 and CdX_2 analogues, so more energy (per degree) is required to bend them.

Not only do the HgX_2 molecules refuse to bend, they apparently do not want to bond, either. This is evident from the long contacts mentioned previously (see values for e in Table 5), and is confirmed in the next section by a quantitative analysis of the (in)stability of the dimers relative to the two monomers from which they are built.

Dimerization energies: The dimerization energy is the energy difference between the M_2X_4 dimers (corrected approximately for basis set superposition errors, BSSE)^[66] and the corresponding pair of isolated MX_2 molecules. E_{dim} is, therefore, the overall change in energy in deforming the optimized MX_2 molecular units for bonding in the dimer (the deformation energy, E_{def} , which always has a cost in energy), and the stabilization upon dimerization. Hence, E_{dim} is negative when the dimer is thermodynamically stable relative to the isolated monomers, and is positive if the dimer is unstable relative to the monomers.

The dimerization energies are listed in columns 5 and 6 of Table 6; they agree very well with the results of Kaupp and von Schnering^[11] for the Zn and Cd dihalides, considering the differences in the applied methods and basis sets. They are somewhat smaller than their energies for the mercury halide dimerizations;^[10] but such small energy differences are inherently less accurate in a calculation. We have also computed the dimerization enthalpies for ZnI_2 and CdI_2 , for which experimental dimerization enthalpies are available. The agreement is not good—but, again, the minute amount of dimers in the vapors at those high temperatures might not be ideal for the experimental determinations.

The E_{dim} values are negative and relatively large for the D_{2h} ZnX_2 and CdX_2 dimers (see column 5 in Table 6). The fluorides form the most stable dimers in both cases, with E_{dim} for Zn_2F_4 (and Cd_2F_4) larger than E_{dim} for Zn_2Cl_4 (and Cd_2Cl_4), for instance, by about 0.40 eV. Among the heavier halides (Cl, Br, and I) the dimerization energies of the Zn_2X_4 and Cd_2X_4 D_{2h} systems are surprisingly similar, with only a slight reduction of about 0.08 eV going from the chlorides to the iodides in both cases (Table 6). The dimerization energy data show that Zn_2X_4 and Cd_2X_4 are quite stable in the D_{2h} geometry. The situation is very different in the Hg systems; there the dimerization energies are all positive (0.17–0.31 eV)—recall that the D_{2h} isomer is only a transition structure for the HgX_2 dimers.

Perhaps more interesting is that even with the relatively insignificant deformation energy required to form the minimum-energy $C_{2h}(1)$ geometry, the overall dimerization energy obtained for Hg_2F_4 (−0.28 eV) is only a quarter of what E_{dim} is for Zn_2F_4 or Cd_2F_4 in their D_{2h} minimum-energy structures. For the larger halides, the Hg_2X_4 dimerization energies are even smaller, decreasing from −0.09 eV in Hg_2Cl_4

to just −0.03 eV in Hg_2I_4 . So, although the Hg_2X_4 $C_{2h}(1)$ deformation energies are quite small, the HgX_2 monomers remain stubbornly unengaging; the very small E_{dim} values attesting to a genuine “thermodynamic disinterest” in dimerization. In the next sections we take a closer look at the unusual bonding pattern in the Hg_2X_4 systems from a frontier molecular orbital perspective. We complement the molecular orbital analysis with a detailed assessment of the ionic contribution to the bonding in the Hg_2X_4 dimers compared to the Zn and Cd cases.

Stretch me if you can: the rigidity of HgX_2 monomers and long contacts in the $C_{2h}(1)$ Hg_2X_4 dimers:

A constrained transit across the potential energy surface of simplified models of the MX_2 dimer helps us to understand the trends observed in Table 6. A series of single-point DFT energy calculations were performed on a representative set of four MX_2 – MX_2 pairs ($\text{M} = \text{Zn}$, and Hg ; $\text{X} = \text{F}$ and I), for different monomer separations. In each case the MX_2 monomers approach each other in a rigidly specified geometry (see inserts in Figure 9). To better understand the preference for the C_{2h} over the D_{2h} dimer geometry by the HgX_2 molecules, we approximated the geometries in the bridges of these dimers in two ways; i) by simply letting two monomers approach each other, keeping r' fixed to the monomer bond length (see Table 1) and ii) setting r' equal to the bridging bond lengths in their optimized D_{2h} structure (see Table 4) which are all longer than the monomer bond lengths by roughly 0.2 Å. Using the monomer bond lengths rather than bond lengths from the $C_{2h}(1)$ dimers is justified since the r' bond lengths in the mercury dihalide $C_{2h}(1)$ dimers are very close to those of the monomer (see Tables 1 and 5). Moreover, the zinc dihalide $C_{2h}(1)$ dimers all collapse to the D_{2h} isomer during optimization so we have no geometrical data for the ZnX_2 $C_{2h}(1)$ dimers (Table 3).

The potential energy curves we obtained for the converging MX_2 – MX_2 pairs are shown in Figure 9a (Zn) and 9b (Hg). The first thing we can notice is that the structure with the longer (D_{2h}) bond lengths (continuous lines in Figure 9a,b) are more stable for all four systems.

It is also obvious that if the bridging bond length is taken as in the D_{2h} optimized structures, the two units can come closer to each other—and this could result in a more stable dimer. This is so even for the HgX_2 dimers (Figure 9b). Why then are the D_{2h} isomers only saddle points for the HgX_2 dimers?

We partitioned the total deformation energy to a stretching and bending part (see Table S14 in the Supporting Information) to see their contribution to the deformation. Apparently, stretching requires a lot of energy; in fact, for the fluorides more so than bending—while for the larger halides the bending is more costly. Stretching the very rigid Hg–X bond requires much too much energy, especially for HgF_2 . An additional large energy is required to bend the molecules—and this seems to be too much, so the HgX_2 molecules prefer the less costly, weak, and loosely bound C_{2h} geometry.

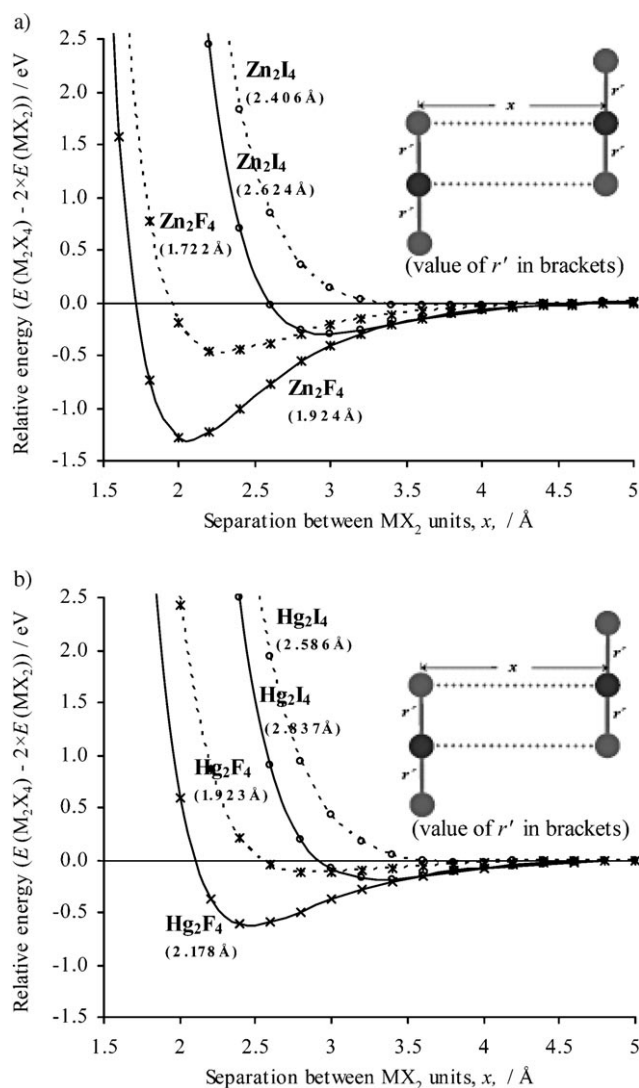


Figure 9. Energy profiles for the direct approach of symmetric MX_2 fragments forming idealized model dimers. (M = a) Zn and b) Hg; X = F and I) with the monomer (-----) and elongated (—) r' values. See text for the basis of our choices of r' .

Frontier molecular orbital interactions between MX_2 fragments: We thought further insight might be obtained from the underlying molecular orbital interactions responsible for the surprisingly long and weak bonding contacts in the minimum-energy $C_{2h}(1)$ structures of the HgX_2 dimers. Figure 10 shows the representations of the key frontier molecular orbitals that would be primarily involved in any side-on ($\text{MX}_2\text{--MX}_2$) bonding of monomers, leading to the D_{2h} or C_{2h} dimers. The $2\pi_u$ MO is the lowest unoccupied π MO, but is just above the $4\sigma_g$ MO in energy (see Figure 4, and Figures S2a–d in the Supporting Information). The $4\sigma_g$ MO is the LUMO in all four of molecules studied.

Figure 10 shows that, as we noted in looking at the σ bonds in Figure 5, the high energy empty np orbitals on the metal are not involved to any significant extent in the occupied MX_2 π MOs either, especially in the Hg systems. The

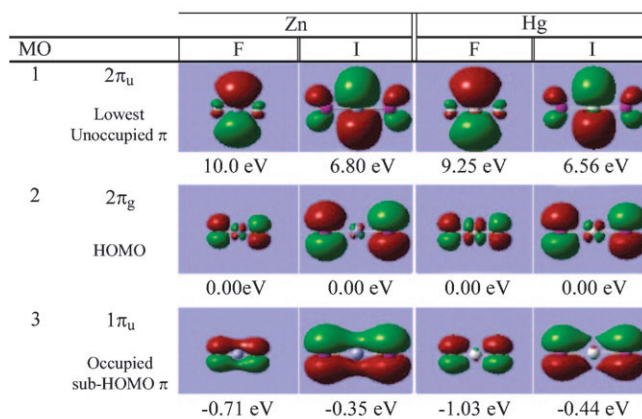


Figure 10. Important MX_2 frontier molecular orbitals involved in stabilizing the M_2X_4 dimers. Only one of each degenerate pair of π MOs (see Figure 4) is shown. The relative energies of the orbitals are also shown.

HOMO π_g and π_u orbitals ((2), and (3) in Figure 10) are made up predominantly of X p contributions, with a substantial input from the metal d orbitals. The unoccupied $2\pi_u$ MO ((1), in Figure 10) is mainly M np , with a small antibonding admixture of X np .

The important frontier orbital interactions are likely to be ones between the occupied $1\pi_u$ and/or $2\pi_g$ (donor) MOs of one MX_2 fragment and the unoccupied (acceptor) $2\pi_u$ MOs—which are much higher up in energy—on the other MX_2 fragment in the M_2X_4 dimer. Schematic depictions of the possible (in-plane σ , and out-of-plane π) interactions between these MOs are shown in Figure 11.

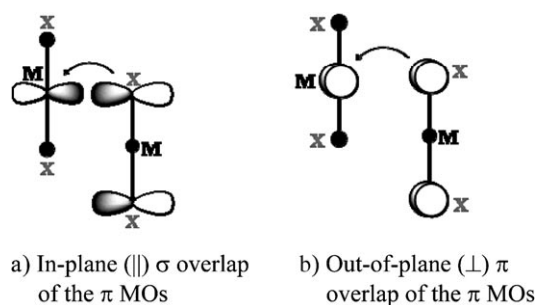


Figure 11. Simplified picture of possible interactions between the degenerate acceptor $2\pi_u$ MO on one monomer and the donor π_u MO (or π_g MO if the p orbitals at the X sites are out of phase with each other) on a partner MX_2 monomer. The arrow indicates the direction of the movement of electrons from donor to acceptor.

The extent of interaction is determined by the energy separation between the two MOs, and their overlap. From a frontier MO perspective, $E_{\text{dim}} \propto |H_{ij}^2|/\Delta E_{ij}$, so the stability of dimers varies roughly as the square of the Hamiltonian H_{ij} (roughly proportional to $-S_{ij}$, the negative of the overlap integral) and inversely with ΔE_{ij} , the energy separation between the two interacting MOs. The energy gaps between the π_g HOMO and the $2\pi_u$ MO are quite large for all the

molecules in Figure 10, so we do not think that ΔE explains the difference in the bonding that we observe.

Orbital interactions, by definition, involve covalent character. Since a number of arguments point to the interpretation that the interaction in the M_2F_4 dimers is largely of electrostatic origin, we looked at the two iodides, in which covalent character is likely to be stronger, for clues. How do the essential frontier orbital overlaps vary when the metal is changed? The DFT computations do not allow easily the calculation of an overlap integral, so we went back to the extended Hückel level to examine the orbital overlaps between the frontier MOs of two fragment MI_2 units in a di-bridged $C_{2h}(1)$ type. The changes in the important in-plane σ orbital overlaps (see Figure 11a), that is, between the $2\pi_g$ and $2\pi_u$ (and between $1\pi_u$ and $2\pi_u$) MOs are plotted in Figure 12 as a function of inter-monomer separation for the two iodides.

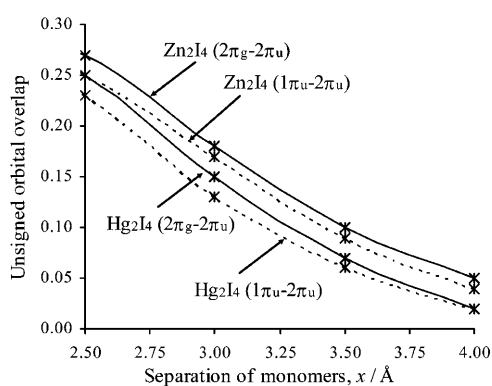


Figure 12. Unsigned σ overlaps as a function of inter-monomer separation, x , for interactions between the acceptor $2\pi_u$ MO on one monomer and the donor $2\pi_g$ (continuous line) and $1\pi_u$ (broken line) MOs on a partner MX_2 monomer.

The orthogonal (\perp) counterparts of the in-plane π MOs overlap with each other as well (in the manner shown in Figure 11b); the overlaps for the (\perp) pairs of MOs are given in Figure S3 in the Supporting Information). As might be expected, the latter π type interactions are relatively insignificant in the bonding region for all four of the molecules we considered.

As seen from Figure 12, the HgI_2 – HgI_2 σ MO overlaps are smaller than the ZnI_2 – ZnI_2 σ MO overlaps. If we compare the overlaps at values of x equal to the optimized bridging distances in Zn_2I_4 and Hg_2I_4 we find that the overlaps are actually much larger in the zinc iodides, about 5 times as large as in the mercury iodides (see Table 7). Thus, for the metal iodides, for which the covalent contribution is the largest, simple frontier orbital interactions do explain the difference between the stability of the Zn_2I_4 and Hg_2I_4 molecules.

Of course, there are other important aspects of the bonding that we have not considered in this simple approach; among them the contributions of other MOs to the population of these orbitals and, more importantly, the electrostatic (attractive and repulsive Coulomb and polarization) interac-

Table 7. Unsigned orbital overlaps for the π MOs in the model zinc and mercury diiodide dimers at physically meaningful inter-monomer separations.^[a]

Monomer	Optimized x [Å] ^[a]	Unsigned orbital overlaps	
		$2\pi_g \leftrightarrow 2\pi_u$ (\parallel)	$1\pi_u \leftrightarrow 2\pi_u$ (\parallel)
ZnI_2	2.624	0.25	0.23
HgI_2	3.655	0.05	0.04

[a] $x = b$ and e (see Tables 4 and 5 for definitions of these distances).

tions between the approaching monomer fragments. These latter interactions will have more and more important role as we go toward the fluorides. Yet, the smaller overlaps for the Hg compounds compared to the Zn compounds in Figure 12 and Table 7 indicate that, compared to the Zn analogues, the HgX_2 MOs are quite inaccessible, requiring unphysical short bonding distances for significant overlap.

Charge distribution: The influence of the “d-block” and “lanthanide” contractions and the relativistic effects on the electronegativity χ and other properties of the Group 12 metals are important in understanding the structural preferences in the MX_2 dimers. One place where the significance of the differences in χ_M is evident is in the charge distribution in the dimer structures.

The NBO charges of the M_2X_4 D_{2h} and Hg_2X_4 $C_{2h}(1)$ dimers are listed in Table 8. The charge separations in the

Table 8. NBO charge and orbital occupancy for the optimized D_{2h} and (for Hg_2X_4) $C_{2h}(1)$ isomers of the Group 12 dihalide dimers.^[a]

MX_2 ^[b]	q [e]			Orbital occupancy at M		
	q_M	$q_{X(b)}$	$q_{X(t)}$	ns	$(n-1)d$	np
relativistic						
D_{2h}						
Zn_2F_4	1.613	−0.828	−0.785	0.37	9.96	0.05
Zn_2Cl_4	1.352	−0.677	−0.676	0.57	9.98	0.08
Zn_2Br_4	1.243	−0.623	−0.621	0.67	9.99	0.09
Zn_2I_4	1.089	−0.555	−0.534	0.79	9.99	0.12
Cd_2F_4	1.593	−0.827	−0.766	0.40	9.95	0.05
Cd_2Cl_4	1.380	−0.707	−0.673	0.57	9.97	0.06
Cd_2Br_4	1.265	−0.643	−0.621	0.67	9.98	0.08
Cd_2I_4	1.129	−0.570	−0.559	0.78	9.99	0.10
Hg_2F_4	1.426	−0.760	−0.666	0.66	9.86	0.04
Hg_2Cl_4	1.181	−0.631	−0.550	0.82	9.93	0.06
Hg_2Br_4	1.067	−0.567	−0.500	0.90	9.95	0.08
Hg_2I_4	0.926	−0.484	−0.442	1.00	9.96	0.10
non-relativistic						
Hg_2F_4	1.625	−0.844	−0.782	0.35	9.96	0.05
Hg_2Cl_4	1.468	−0.755	−0.713	0.49	9.98	0.06
Hg_2Br_4	1.368	−0.701	−0.667	0.57	9.98	0.07
Hg_2I_4	1.235	−0.628	−0.607	0.68	9.99	0.09
relativistic						
$C_{2h}(1)$						
Hg_2F_4	1.358	−0.704	−0.654	0.81	9.78	0.04
Hg_2Cl_4	1.112	−0.575	−0.536	0.94	9.88	0.06
Hg_2Br_4	1.010	−0.523	−0.487	1.00	9.90	0.04
Hg_2I_4	0.884	−0.458	−0.427	1.08	9.93	0.09

[a] M = metal, X(b) = bridging halogen, X(t) = terminal halogen.

[b] For the non-relativistic calculations we employed the MHF ECP and basis set for Hg. The molecular formula is in bold in the case where the isomer is the (relativistic) minimum-energy structure.

M–X bonds of the D_{2h} dimers are similar for Zn, and Cd, but are always smaller for Hg. In the preferred $C_{2h}(1)$ geometry the charge separation is even smaller than in the D_{2h} isomer. This general pattern was observed in the monomeric MX_2 molecules as well, consistent with the variation in χ_M : $\chi_{Zn} \approx \chi_{Cd} < \chi_{Hg}$, largely caused by significant relativistic effects on Hg.

Comparison of the NBO charges on the metal atoms in the monomers and dimers shows a noticeable increase in the dimers (e.g., by about $0.08e$ in ZnF_2 down to about $0.02e$ in ZnI_2 , see Tables 2 and 8). Similarly, the NBO charges on the bridging halogen atoms are considerably larger than those of the terminal halogens in each dimer. This suggests that the formation of dimers is primarily driven by electrostatic forces.

In the Hg_2X_4 D_{2h} structures the same situation is observed, with an even larger charge increase on the metal ($0.11e$ and $0.06e$ in HgF_2 and HgI_2 , respectively) and the bridging halogens. For the minimum-energy $C_{2h}(1)$ structures this charge increase is much smaller ($0.05e$ and $0.02e$ for HgF_2 and HgI_2 , respectively), but still present. We can imagine that with the relativistically stabilized $6s$ electrons this charge transfer from the metal to the bridging halogen is becoming more and more costly energetically. This could be one of the reasons that the mercury halides favor the relatively less costly $C_{2h}(1)$ arrangement.

As we observed for the charge density in the monomers (vide supra), the np orbital occupancy in the minimum energy dimer structures (see Table 8) is effectively zero. This situation is observed in the non-relativistic dimer calculations as well, see the Hg_2X_4 structures in Table 8. The non-involvement of the p orbitals in bonding can be explained by the relatively large s – p energy gap, observed experimentally for the Group 12 atoms (Figure 1). This energy gap is especially large for Hg and that makes the hybridization necessary for bending quite expensive. The poor overlap between the Hg np orbitals and the halide lone pairs leads to the loose contacts in the HgX_2 dimers. Beside these arguments, the considerably increased metal charges in the D_{2h} dimers versus the small charge separation in Hg–X bonds (due to relativistic effects), do not make the formation of D_{2h} dimers viable and are all responsible for the tendency of mercury halides to form the $C_{2h}(1)$ symmetry dimers, in which the charge transfer is smaller.

Gold halide and mercury halide dimers—a stunning difference

At the end of this discussion of the dimers, a comparison of dimerization tendencies and the stability of bridging bonds in gold and mercury halide dimers is instructive. Gold and mercury are often mentioned together as the most obvious examples for displaying the consequences of relativistic effects, either purely as a metal or in their compounds. In this regard, it is remarkable, how everything about their dimers differ (here we refer to the Au_2X_2 and Hg_2X_4 dimers). For AuX , dimerization is exothermic for all halides and increas-

ingly so toward the iodides ($E_{\text{dim}} = -1.06$ and -1.66 eV for AuF and AuI , respectively [CCSD(T) values, not corrected for BSSE]).^[67] As we saw above, HgX_2 molecules seem to resist dimerization and only form loosely bound systems—with their dimerization energy decreasing (and not increasing as for AuX) toward the iodides ($E_{\text{dim}} = -0.28$ and -0.03 eV for HgF_2 and HgI_2 , respectively). So, while E_{dim} increases about 60 % from AuF to AuI , for the mercury halides E_{dim} of HgI_2 is a mere tenth of that of HgF_2 . How do we explain this very different behavior?

The gold monohalide dimers are stabilized by a strong metallophilic interaction (they even earned their own *appellation*: *aurophilic* interaction) that is especially strong with soft ligands, and therefore this effect increases toward the iodides (see ref. [68]). This is indicated by the decreasing Au···Au distance in the dimers (2.951 vs. 2.792 Å for AuF and AuI , respectively, for AuI this is shorter than the Au–I bond length, 2.807 Å).^[67] This metallophilic interaction, on the other hand, is less likely to play a role between the mercury atoms, due to their increased positive charge (q_M on Au changes from $0.65e$ to $0.41e$ in Au_2X_2 from F to I, while the same for Hg_2X_4 changes from $1.36e$ to $0.88e$). In the absence of the metallophilic interaction, the dimerization in HgX_2 is directed by electrostatic forces (however weak these may be relative to the Zn and Cd cases), and this explains why the Hg_2F_4 dimer is the most stable among the mercury dihalide dimers.^[69]

The significance of the electrostatic interaction between the HgF_2 monomers compared to the other HgX_2 molecules shows up again in a rather more dramatic fashion in the extended solids of the mercury dihalides. In the next section we analyze the structural preferences in the Group 12 dihalide extended solids.

Group 12 dihalide extended solids

As mentioned previously, the Group 12 dihalide extended solids exhibit a diverse set of structure types at ambient conditions as seen in Figure 13. Table 9 shows the crystal structures that each of the Group 12 dihalides adopt.

ZnF_2 has the well-known rutile (TiO_2) structure with CN = 6 at the Zn sites. The heavier Zn dihalides show a preference for lower-coordination (CN = 4) extended solid structures. The α - $ZnCl_2$ structure is a three-dimensional array of edge-sharing $ZnCl_4$ -tetrahedra. The $ZnBr_2$ and ZnI_2 extended solids are isotypic, having a structure that may be described as a three dimensional system of interconnected $Zn_4X_6X_{4/2}$ supertetrahedra ($ZnBr_2$ structure type; see ref. [70]).

Almost all the CdX_2 extended solids have a stable six-coordinate layered structure—the $CdCl_2$ structure type (for $CdCl_2$ and $CdBr_2$) and the CdI_2 structure. CdF_2 is an exception, taking instead the eight-coordinate fluorite (CaF_2) structure type. HgF_2 has the fluorite structure, as well, which makes it the only structure in the HgX_2 series with CN > 4.^[71] $HgCl_2$ and $HgBr_2$ are molecular-type solids, each with a different stacking of linear MX_2 units (CN = 2). HgI_2 is a

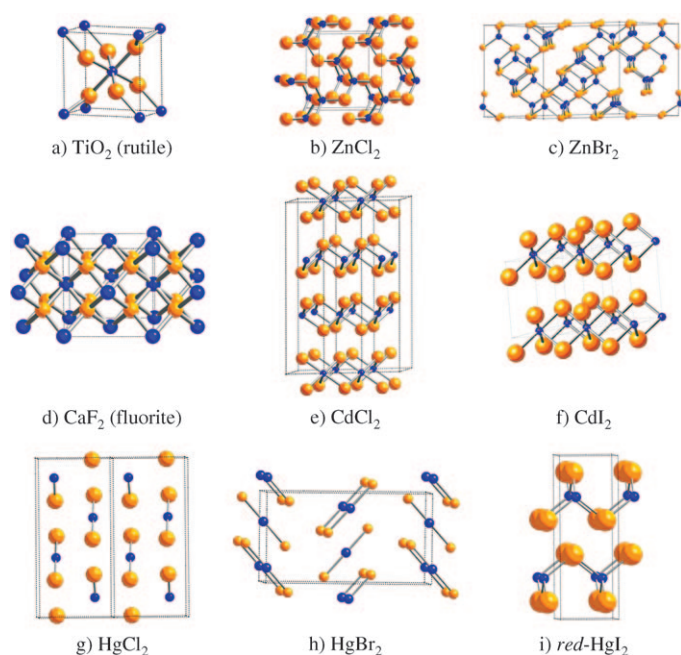


Figure 13. Structure types of the Group 12 metal dihalide crystals.

Table 9. Structural preferences in the Group 12 dihalide monomers, dimers, and extended solids and coordination numbers (CNs) in the solids at ambient conditions.

		F	Cl	Br	I
Zn	molecular structure	linear	linear	linear	linear
	dimer structure	D_{2h}	D_{2h}	D_{2h}	D_{2h}
	solid structure type	TiO_2	$\alpha\text{-ZnCl}_2$	ZnBr_2	ZnBr_2
Cd	molecular structure	linear	linear	linear	linear
	dimer structure	D_{2h}	D_{2h}	D_{2h}	D_{2h}
	solid structure type	CaF_2	CdCl_2	CdCl_2	CdI_2
Hg	molecular structure	linear	linear	linear	linear
	dimer structure	C_{2h}	C_{2h}	C_{2h}	C_{2h}
	solid structure type	CaF_2	HgCl_2	HgBr_2	$\text{HgI}_2^{[a]}$
	coord. no. in solid	8	2	2	4 ^[a]

[a] Red- HgI_2 (CN=4) is the most stable at ambient conditions, but a few forms of orange HgI_2 and a yellow polymorph of HgI_2 (CN=2) are also known (ref. [71]).

polymorphic solid, one form of which (yellow- HgI_2 , stable above 126°C) is isotopic with the HgBr_2 structure. At ambient conditions, however, another polymorph (red- HgI_2), made up of layers of edge-sharing tetrahedra (CN=4), is the most stable form. Clearly HgI_2 lies close to a molecular/extended solid borderline.

Link to structural preferences in the monomers and dimers

In our study of the Group 2 dihalide molecules and solids we observed that in general, the linear (bent) molecules form minimum energy D_{2h} (C_{3v}) dimer structures and condense to form low coordination, $\text{CN} \leq 6$, (higher coordination, $\text{CN} > 7$) solids at ambient conditions. An analysis of

the structural preferences in the Group 12 dihalide monomers, dimers, and solids (summarized in Table 9) shows some correspondence to the situation in the Group 2 dihalides, as well as some extraordinary differences.

In the previous sections of this work, we have confirmed the rather monotonous structural preferences in the Group 12 dihalide monomers (which are all linear) and their dimers (which all prefer a doubly bridged D_{2h} or C_{2h} geometry). So, with the results from the linear Group 2 dihalides as a reference, at a first glance we might have expected relatively low coordination numbers, $\text{CN} \leq 6$, for the extended solids of all the Group 12 dihalides. This is observed for ten of the twelve Group 12 dihalides, but it would be dangerous to draw the conclusion that the reasons for the particular structures are necessarily the same in the Group 12 compounds as they are for the Group 2 compounds.

We might start our comparison with the Group 2 dihalide solids by remembering that there is one important difference between the two groups; and that is the condition of the $(n-1)d$ orbitals; empty in the Group 2 and filled in the Group 12 dihalides. It has been discussed in reference [1] that the availability of these empty d orbitals is one of the reasons for the sometimes unexpected structures of their dihalides, be it monomers, dimers, or solids. This is not the case for the Group 12 dihalide molecules and we already saw that, indeed, their monomers and dimers behave quite differently from the Group 2 dihalides.

Structure preferences in the fluorides: There are two Group 2 metals in which there are no empty $(n-1)d$ orbitals; Be and Mg. Beryllium is too small a cation to be compared with the Group 12 metals, and that leaves us with Mg. MgF_2 has a rutile-type structure with 6 coordination of the metal—so does ZnF_2 . The ionic radii of Mg and Zn are very close ($\approx 0.72 \text{ \AA}$ and $\approx 0.74 \text{ \AA}$, respectively), so that the cation/anion (M^{2+}/F^-) radius ratio for $M=\text{Mg}$ and Zn are almost identical. Although the electronegativity of the Group 12 metals is larger than that of the alkaline earth metals, the electronegativity difference between the metal and the fluorine is large enough, even with Zn, to give an ionic crystal.

The similarity between the magnesium dihalides and the Group 12 dihalides goes further. The other magnesium dihalides have the cadmium dihalide structures, again, with $\text{CN}=6$. This, in fact, might be surprising, since the cation/anion radius ratio for the MgX_2 dihalides ($X=\text{Cl}, \text{Br}, \text{I}$) is smaller than 0.414—and thus, according to Pauling's ionic radius ratio law,^[72] they should rather have tetrahedral coordination.^[73]

Continuing with the fluorides, the crystal structures of CdF_2 and HgF_2 are surprising if we follow the logic established for the Group 2 dihalides; while the CaF_2 monomer is bent, both CdF_2 and HgF_2 are linear molecules—still they all have the same crystal structure with $\text{CN}=8$. The preference in CdF_2 and HgF_2 for the ionic (fluorite) extended solids may be rationalized, in part, by the radius ratios of the metal cation and the fluoride ions. The ionic radii of the

Cd^{2+} and Hg^{2+} cations ($\approx 1.10 \text{ \AA}$ and $\approx 1.14 \text{ \AA}$, respectively) are relatively close to each other and to the radius of the Ca^{2+} cation ($\approx 1.12 \text{ \AA}$).^[74,75] So, a preference in CdF_2 and HgF_2 for the (CaF_2) fluorite structure type should not be surprising, based simply on radius ratios alone. The cation/anion radius ratios of about 0.83 and 0.86 for CdF_2 and HgF_2 , respectively (for F^- radius = 1.33 \AA), call for an 8-coordination of the metals according to Pauling's rule (similarly to CaF_2 with a ratio of 0.84).

Yet, it would be too simplistic to base our arguments on radius ratios alone, after all, there are considerable differences between CaF_2 on the one hand, and CdF_2 and HgF_2 , on the other. To have a purely ionic solid, substantial difference between the electronegativities of the metal and the halogens is expected. How does this look for the CaF_2 , CdF_2 and HgF_2 fluorite systems? The electronegativity difference between M and F is larger for Ca ($\Delta\chi = 8.2$ —remember, we are using absolute Mulliken electronegativities)^[55,56] than it is for Cd ($\Delta\chi = 6.1$) and Hg ($\Delta\chi = 5.5$). So, although CaF_2 , CdF_2 and HgF_2 all adopt the ionic fluorite structure at ambient conditions, the CdF_2 and especially the HgF_2 fluorite structures are expected to be less ionic than the CaF_2 fluorite structure.

We envisage, in fact, that had the relativistic effects caused an even larger increase in χ_{Hg} such that $\Delta\chi$ was smaller (in other words, if the charge shift in the $\text{Hg}-\text{X}$ contacts in the solid was reduced), *with the Hg^{2+} ionic radii unchanged*, the fluorite structure would be disfavored. The ratio of the Hg^{2+} and F^- radii and other packing forces favor the fluorite structure, and overcompensate for the destabilizing influence of the decrease in $\Delta\chi$ on going from Ca to Cd and Hg. So, in the Group 12 difluorides the increased electronegativity of the metal ions (increasing covalent character of the bonding in the solids^[76]) fails to enforce a more covalent structure type.

However, the diminished $\Delta\chi$ in the Group 12 difluorides, compared to the magnesium and calcium difluorides, is apparent in the differences in the melting points of the isotopic Group 2 and Group 12 solids. As Table 10 indicates, the melting points of the Group 12 difluorides are noticeably lower than those of the isotopic dihalides of Group 2 metals of similar ionic radii.

Still, for one particular reason, the choice of the fluorite structure for CdF_2 and HgF_2 might be surprising, and that is the rigidity of the linear monomer units in the gas phase.

The HgF_2 molecule is exceptionally rigid (see Figure 3a) and the bonding between the two almost linear HgF_2 units in the dimers is exceptionally weak. So we might have been deceived into thinking that the continued agglomeration of HgF_2 units, so loosely bonded in the dimer, would give eventually a molecular solid. *But a curious thing happened on the way to the solid. As more fluorides coordinate to the Hg, it appears that an ionic switch is turned on. The intensified and increasingly isotropic electrostatic field seems to promote delocalization of the electron density out of the bonds of individual HgF_2 units (a removal of bond directionality as suggested in reference [51b]) and consequent strengthening of $\text{Hg}-\text{F}$ interactions among individual monomer units.*

The way this “ionic progression” occurs, and where in the oligomerization (or, at what cluster size) it becomes dominant, are not completely understood. The fact that already in the dimers the metals and the bridging halogens both become more ionic (compare q_{X} and $q_{\text{X(b)}}$ in Tables 2 and 8) than they are in the monomer, is a sign of this progression. We intend to consider those questions further in separate discussions. It is apparent, however, that the electronegativity of X is decisive for the gradual move from the weakly bonded dimer to the ionic solids, since no ionic solid is known for the heavier dihalides ($\text{X} \neq \text{F}$) of Hg.

Structure preferences in the heavier halides: The heavier Zn dihalides ($\text{X} = \text{Cl}, \text{Br}, \text{I}$) all have tetrahedral coordination in their solids, as mentioned above, and with that they all obey the Pauling radius ratio rule^[72] (they are between 0.33 and 0.27 for the three ZnX_2 molecules^[77] and are thus within the range (0.23–0.41) given for tetrahedral arrangements). The decrease in $\Delta\chi_{\text{M-X}}$ does not have such a strong effect as to override it. The CdX_2 solids ($\text{X} = \text{Cl}, \text{Br}, \text{I}$) have layer structures with octahedral metal coordination. The cation/anion radius ratios correspond to this (they are between 0.52 and 0.43)—but the electronegativity differences between the metal and the halogens are getting smaller. This leads to the decreasing ionic character of these solids as shown, again, by their lower melting points compared to the MgX_2 and CaX_2 solids, all with CN=6 (see Table S15 in the Supporting Information).

In the mercury chlorides, bromides and iodides the difference in electronegativity between the atoms in the $\text{Hg}-\text{X}$ bond is even smaller. As a consequence, the approach of more molecules in the crystal cannot anymore induce the delocalization of electron density. Thus ionic structures are no longer stable for these solids. In those compounds the similarity in the metal radii (of Ca and Hg) is no longer decisive for the structure-type preferences, as is the case in the fluorides. The diminished ionicity (increased covalency) in the $\text{M}-\text{X}$ contacts causes lower coordination and, for HgCl_2 and HgBr_2 , even molecular extended solids to be preferred.

Let us compare the structural preferences in the chlorides and bromides of Ca and Hg. CaCl_2 and CaBr_2 both have three-dimensional six-coordinate structures (CaCl_2 structure type) that are closely related to the rutile structure. HgCl_2 and HgBr_2 , on the other hand, are two-coordinate molecular

Table 10. Melting points of the rutile and fluorite structures of Groups 2 and 12 difluoride extended solids with M^{2+} ions of comparable ionic radii.^[a]

Structure type	Melting points [$^{\circ}\text{C}$]			
	Group 2		Group 12	
rutile	MgF_2	1263	ZnF_2	872
fluorite	CaF_2	1418	CdF_2	1075
			HgF_2	645 ^[b]

[a] Melting temperatures are taken from ref. [74], Section 4, pp. 43–101.

[b] Decomposes.

solids. So the influence of the increasing covalence going from CaX_2 to HgX_2 —that already appeared in the fluorides but could not yet overcome the effect of ideal radius ratios—becomes evident in the dichlorides and dibromides—and in the polymorphs of the iodides, as well.

Lower coordination in mercury: The different possible reasons for the preference for two coordination in mercury compounds are discussed in reference [10]. Nyholm^[78] suggested that the preference for a low coordination at Hg in its molecules is explained by the large s–p energy gap. Our results, like those of Kaupp and von Schnering,^[10] support this observation, just as they do those of Orgel.^[79] Orgel, prior to Nyholm's work, explained the preference for low coordination in Hg compounds by an important $ns-(n-1)d$ hybridization for the Hg cation in the HgX_2 dihalides. In a qualitative assessment of the stabilities of Hg^{2+} compounds with the Hg^{2+} in a six-coordinate octahedral versus a two coordinate environment, Orgel concluded that where the $ns-(n-1)d$ gap is sufficiently small, the d and s orbitals can mix to give a $d^{10-\delta}-s^\delta$ configuration in which the s and d_{z^2} orbitals are hybridized.^[79] This would preferentially stabilize a distorted octahedral configuration with the two axial bonds much shorter than the equatorial bonds, that is, a distortion from the octahedral to an effectively linear (two-coordinate) environment for the metal.

This rationalization is compatible with the arrangement of the HgX_2 units in the molecular solids of HgBr_2 , for example, in which equatorially positioned halides are identifiable outside the two-coordinate nearest neighbor shell (see, for example, Figure 1 in ref. [10]). Our observation of a somewhat larger charge shift from the $(n-1)d$ orbital of the metal to the M–X bond (of the monomers and dimers) for Hg compared to the Zn and Cd analogues is in line with a greater participation of the d orbitals in the mercury halides. This happens in both the HgX_2 monomers and dimers—well before any significant aggregation on way to the solids.

Kaupp and von Schnering have pointed out that the relativistic increase in the electronegativity of Hg itself is a key factor in the preference for a lower coordination.^[10] The reduced charge displacement (or increased covalence) in the Hg–X bond discourages high coordination in both the molecules and the solids. Nonetheless, when X is sufficiently electronegative the charge shifts in the Hg–X bonds may be enough to dominate over these covalent effects—as in the CdF_2 and HgF_2 solids, where we get perforce into the ionic regime.

Kaupp and von Schnering also suggested that repulsion between the electrons in the relativistically destabilized (expanded) $(n-1)d$ orbitals of the Hg atom in one monomer unit and the charge density of neighboring monomers may hinder oligomerization.^[10] However, the high coordination in the HgF_2 (fluorite) solid, which has the shortest Hg–X contacts between monomer units, implies that repulsion between the X lone pairs and the Hg $(n-1)d$ electron density is insignificant, compared to the other interactions influencing structural outcomes in the HgX_2 solids.

In the molecular crystal of HgCl_2 , the shortest distance between chlorine atoms of neighboring molecules is smaller than the sum of the van der Waals radii of chlorine, suggesting attractive $\text{Cl}\cdots\text{Cl}$ interactions.^[71,80] For HgCl_2 , HgBr_2 , and the polymorphs of HgI_2 the application of high pressure brings some of the molecular units with weak attractive van der Waals interactions close to each other and may even induce bending of the X–M–X unit in the molecular solids or induce aggregation. A high-pressure phase of HgCl_2 (structure IV in ref. [71]) is a series of bent HgCl_2 molecular units; for HgI_2 an increase in pressure (structure VI in ref. [71]) forces the formation of Hg_2I_4 C_{2h} dimeric units with relatively long contacts reminiscent of the C_{2h} -symmetry relativistic dimer structures discussed earlier. The phase diagrams of the mercury dihalides show different structural preferences in general as a function of X, despite the similarities between some of the bromide and iodide structures.

The halide factor: relative stabilities of the HgX_2 structure types for different halides:

The structural preferences of the different mercury dihalide extended solids at ambient conditions are well known (see Figure 13 above) and even their phase diagrams, except that of HgF_2 , have been studied in detail.^[71] At slightly elevated temperatures and pressures^[81] the number of known polymorphs increases dramatically with increasing halogen size. Hostettler and Schwarzenbach identified nine stable and metastable polymorphs for HgI_2 —including the red, yellow, and orange structures mentioned above—compared to only four polymorphs for HgCl_2 (all molecular solids) and three for HgBr_2 .^[71] No alternative to the fluorite structure has been identified for HgF_2 at ambient conditions. As for competitive polymorphs at elevated temperatures and pressures, difficulty in preparing pure dry HgF_2 samples (see ref. [71]) has inhibited the mapping out of a phase diagram for this compound.

What alternative polymorphs of HgF_2 are likely to exist far from ambient conditions (at high pressures, for instance)? All the other mercury dihalides have stable molecular crystals, even if, as in the case of HgI_2 , they are not preferred at ambient conditions; might HgF_2 also have such a structure? To answer this question in detail would take us well beyond the scope of this work. Nonetheless, we take a small step here to begin to respond to this question. We investigate, for each of the four HgX_2 compounds the stability of their preferred crystal structure relative to the crystal structures adopted by the other three HgX_2 compounds at ambient conditions.

The hypothetical analogues of the experimental HgCl_2 , HgBr_2 , and (red) HgI_2 structures in which the halides (X = Cl, Br, and I, respectively) are replaced by fluorine were each optimized under constraints: the fractional coordinates of the ions in the experimental structure, and the cell shape (the axial ratios) were unchanged while the cell volume was optimized (using the VASP program; see the Theoretical Methods section). A similar set of calculations were performed for the other three halides; the results of the calculations are summarized in Figure 14.

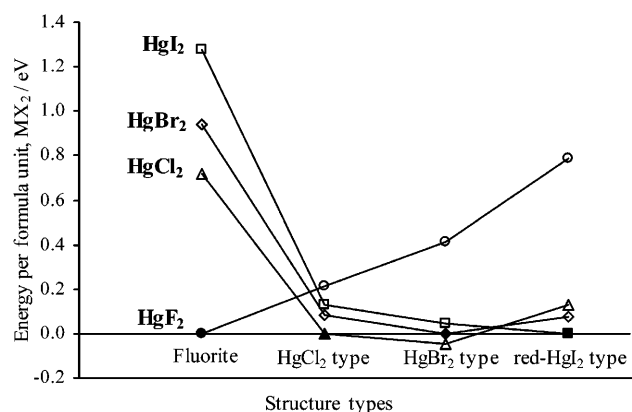


Figure 14. Relative energies of hypothetical HgX_2 crystal structures. For each compound, the actual extended solid structure at ambient conditions is indicated by a solid black label.

Mercury difluoride shows a definite preference for the three-dimensional fluorite structure over the alternative structures adopted by the heavier halides; the structure type closest in energy to this is the hypothetical molecular HgCl_2 structure type (see the HgF_2 line in Figure 14). Note that the two-dimensional red- HgI_2 in which the halides are more highly coordinated is the least favored of the four structure types for HgF_2 . This may be explained by a significant degree of reorganization that would be necessary to move to the red- HgI_2 structure compared to the HgCl_2 structure. In the HgCl_2 structure-type the Hg sites may be described as 2+6 coordinated, with the six atoms quite far away from the Hg.^[80] A reduction of these six long Hg–Cl distances would generate an eight-coordinated Hg site which could symmetrize to give the cubic environment in which Hg in the fluorite structure sits. In fact, we have observed in our calculations, quite by accident, that this structural transition occurs readily if HgF_2 in the HgCl_2 structure type is optimized without constraints.

The rejection by HgF_2 of the other HgX_2 structure types is strongly reciprocated by the other three mercury dihalides. Notice the wide gap above the fluorite column in Figure 14 separating the stable HgF_2 solid from the high-energy hypothetical fluorite incarnations HgCl_2 , HgBr_2 , and HgI_2 . The fluorite structure is extremely unstable (by ≈ 0.7 eV to 1.4 eV) relative to the other three structure types for the larger halides. For HgBr_2 and HgI_2 our results affirm the preference of these compounds for the structure types that is observed at ambient conditions. For HgCl_2 we obtained slightly greater stability in the HgBr_2 molecular structure type (≈ 0.05 eV) than in the actual HgCl_2 structure type, but the small, ≈ 0.05 eV energy difference is well within the uncertainties in the energy values. Moreover, the HgCl_2 and HgBr_2 structure types are close in energy for all the dihalides except HgF_2 . HgI_2 is known to have a metastable polymorph with HgBr_2 structure type; but HgCl_2 has not been observed so far in the HgBr_2 structure type.

Admittedly, we are trying something risky here, using DFT for both molecular and extended structure calculations.

The equilibrium geometries of the latter are set by van der Waals interactions, the former by covalent and ionic bonding. There is ample evidence that (to put it mildly) it is hard to get functionals that work in all bonding regimes. In a way, it is surprising (and gratifying) that the computational results seem as reasonable as they are.

Summary

In this paper we identify connections between the structures of Group 12 dihalides in different stages of aggregation—from the monomers to dimers and on to the extended solids. In this endeavor we were encouraged by the remarkable links we found among the structures of monomers, dimers and crystals of the Group 2 dihalides.^[1]

In the course of our work we learned that even though it is generally accepted that the Group 2 and 12 metal dihalides, with their metals having oxidation number 2 in both cases, are very similar—chemistry is more subtle. Indeed, we found some interesting similarities between the two groups; but the differences are more striking.

The dissimilarities start right away with the structure of the monomers: while the Group 2 dihalides have both linear and bent (and quasilinear) geometries, the Group 12 dihalide monomers are all linear. It is primarily the difference in the occupation of the $(n-1)d$ orbitals of the metals that is responsible for this; these orbitals are empty in Group 2 and completely filled in the Group 12 dihalides. There are other differences in the structures of the two groups of monomers, due to the difference in the positions of the two groups of metals in the periodic table. The radii of Group 12 atoms are much smaller than those of the alkaline earth metals. For mercury this is a well-known relativistic effect. As a result, the electronegativities of the Group 12 metals are larger than those of the alkaline earth metals. Similarly, the energy gap between the ns and np orbitals is much larger in the Group 12 metals than in the alkaline earth metals—leading to differences in the structures of their dihalides.

While geometrical and electronic properties in the Group 2 dihalide monomers change monotonously down the column of the periodic table, among the Group 12 dihalides mercury is an exception. Most of the properties of Hg systems deviate sharply from patterns set by the Zn and Cd analogues—due chiefly to the strong relativistic effect on the mercury atom. The electronegativity of Hg is larger than that of Zn and Cd and, consequently, the charge separation in the Hg–X bond is smaller than in the Zn and Cd analogues; also the Hg–X bonds are shorter than the Cd–X bond lengths.

An important characteristic of the Group 12 dihalides and especially of the mercury dihalides is their rigidity—a feature that has consequences on the structure of the dimers as well. As shown in references [1,15,23,24], the bending force constant of the alkaline earth dihalides decreases down the group, as it is easier to polarize the larger metal atoms. The bending force constants of the ZnX_2 and CdX_2 molecules

are much larger than those of the Group 2 dihalides. And the HgX_2 molecules are exceptionally rigid—they resist both stretching and bending as a result of the large relativistic contraction of their s orbitals. An important feature of the mercury dihalides is the participation of the filled $(n-1)d$ orbitals in bonding; relativistic effects destabilize these orbitals and they need to be considered as part of the valence shell of these systems.

There is a clear connection between the structures of the monomers and dimers in the Group 2 dihalides: all linear monomers form D_{2h} -symmetry dimers and all bent monomers form a dimer with C_{3v} symmetry.^[1,64] In Group 12, the Zn and Cd dihalides—similarly to the linear alkaline earth dihalides—form D_{2h} -symmetry dimers. However, their dimerization energies are considerably smaller (by 0.5 eV to 1.5 eV) than those of the Group 2 dihalides (except for the beryllium dihalides, which behave differently, due to the very small size of beryllium); the reason may be the non-availability of empty d orbitals and the lower degree of ionicity in the Group 12 dihalides. This difference also explains the low dimer contents in the vapors of Group 12 dihalides, which prevents the experimental determination of their structures. This is in contrast to the Group 2 dihalides; most of their dimers were detected in gas-phase structural studies.^[12]

The HgX_2 dimers are different both structurally and energetically—and this can be traced back to the peculiarity of their monomers. They have a much more rigid linear framework, resisting both bending and bond stretching, than the Zn and Cd dihalides. Therefore, the mercury compounds form loosely bound C_{2h} -symmetry dimers, in which the mandated bending, the charge separation in the original M–X bond, and the charge increase on the metal and bridging halogen atoms are all minimized. The dimerization energy of HgX_2 molecules is especially small, for all X (0.28 eV for HgF_2 and less than 0.1 eV for the rest). That the HgF_2 dimer is more stable than the other HgX_2 dimers supports the idea that dimerization in these systems is directed by electrostatic forces.

The crystal structures of Group 12 dihalides exhibit an impressive array of structure types, from extended three-dimensional structures to layers and to molecular solids. This is in contrast with the Group 2 dihalides, which generally have ionic three- or two-dimensional structures. Could the availability of empty $(n-1)d$ orbitals play a role here? Not counting the beryllium compounds, Mg is the only Group 2 metal that does not have an empty $(n-1)d$ orbital. Do then its dihalides have similarity with their Group 12 counterparts, the zinc dihalides? Indeed, they do, for all their dihalides, as discussed in the previous section.

CdF_2 and HgF_2 have the CaF_2 (fluorite) crystal structure. This might seem especially surprising for HgF_2 , for which the charge separation in its monomer is the smallest. However, even though mercury holds on to its electrons more than the other elements in the group, the approach of more molecules with their electronegative fluorines eventually outweighs this. The mercury lets its electrons go—and the

system becomes an ionic solid. The fact that the partial charges of the Hg and the bridging F atoms in the C_{2h} dimer are larger than in the monomer molecule already suggests this. The crystals of HgCl_2 and HgBr_2 are molecular solids. Apparently, the less electronegative ligands cannot draw away electron density from the Hg atom; thus extended structures cannot be formed. The participation of the $(n-1)d$ electrons in the valence shell also favors the linear structure, as suggested earlier.^[79]

It was reassuring to see that for all molecules in the group there is a clear connection between the preferred structure and the electronic character of monomers, dimers and, eventually, the crystals that they form. Among the Group 12 dihalides, the peculiarity of the mercury dihalides is apparent. In all types of aggregation, the structures of its dihalides are different from the rest of the dihalides—and this can be traced back to relativistic effects on Hg. All other characteristics of mercury in its compounds, such as the metal's increased electronegativity, decreased charge separation in its bonds, shorter bond lengths, exceptionally large $ns-np$ orbital gap, participation of $(n-1)d$ orbitals in bonding; and the fact that it is mostly electrostatic interactions that are responsible for forming oligomers and eventually their crystals—all of these are a consequence of relativity.

Acknowledgements

A significant part of this work was completed while K.J.D. was a research associate at Cornell University, Ithaca, N.Y. The bulk of the calculations were performed on the Intel Cluster at the Cornell Nanoscale Facility, which is part of the National Nanotechnology Infrastructure Network (NNIN) funded by the National Science Foundation (NSF). For supporting the research at Cornell we thank the National Science Foundation, Grant CHE-0613306. We are grateful to J. Feng and P. Gonzales-Morelos for help with computational resources and J. von Appen, R. Dronskowski, and P. Kroll for insightful discussions and advice. K.J.D. acknowledges the University of Richmond and the Department of Chemistry for support. M.H. thanks the Hungarian Scientific Research Fund (OTKA K 60365) for support.

- [1] K. J. Donald, R. Hoffmann, *J. Am. Chem. Soc.* **2006**, *128*, 11236.
- [2] N. N. Greenwood, A. Earnshaw, *Chemistry of the Elements*; Pergamon Press: Oxford, 1st ed, **1990**, pp. 1400–1403.
- [3] P. Pykkö, *Chem. Rev.* **1988**, *88*, 563.
- [4] W. H. E. Schwarz in *Fundamentals of Relativistic Effects in Chemistry, in Theoretical Models of Chemical Bonding, Part 2: The Concept of the Chemical Bond* (Ed.: Z. B. Maksic), Springer, Berlin, **1990**, pp. 593–643.
- [5] N. N. Greenwood, K. Wade, *J. Chem. Soc.* **1956**, 1527.
- [6] P. Pykkö, *J. Chem. Res.* **1979**, *11*, 380.
- [7] For a brief overview of the d-block contraction and factors counterbalancing this contraction in period 5, see ref. [3], pp. 565–567.
- [8] P. S. Bagus, Y. S. Lee, K. S. Pitzer, *Chem. Phys. Lett.* **1975**, *33*, 408.
- [9] Relativistic effects in the atom include, simplistically, a) an increase in mass of the high speed core electrons, in particular the lowest energy s and p electrons, which, in turn, causes a reduction in the radii of these orbitals. Consequently, the higher s and p energy orbitals adjust and contract as well to ensure orthogonality; b) spin-orbit coupling and c) a destabilization and expansion in space of the outer d and f orbitals due to the contraction of the s and p orbitals.
- [10] M. Kaupp, H. G. von Schnering, *Inorg. Chem.* **1994**, *33*, 2555.

- [11] M. Kaupp, H. G. von Schnering, *Inorg. Chem.* **1994**, 33, 4718.
- [12] M. Hargittai, *Chem. Rev.* **2000**, 100, 2233.
- [13] a) L. Wharton, R. A. Berg, W. Klemperer, *J. Chem. Phys.* **1963**, 39, 2023; b) A. Büchler, J. L. Stauffer, W. Klemperer, *J. Chem. Phys.* **1964**, 40, 3471; c) A. Büchler, J. L. Stauffer, W. Klemperer, *J. Am. Chem. Soc.* **1964**, 86, 4544.
- [14] L. von Szentpály, P. Schwerdtfeger, *Chem. Phys. Lett.* **1990**, 170, 555.
- [15] M. Kaupp, P. von R. Schleyer, H. Stoll, H. Preuss, *J. Am. Chem. Soc.* **1991**, 113, 6012.
- [16] M. Kaupp, *Angew. Chem. Int. Ed. Engl.* **2001**, 40, 3535, and references therein.
- [17] P. Garcia-Fernandez, I. B. Bersuker, J. E. Boggs, *J. Phys. Chem. A* **2007**, 111, 10409.
- [18] C. A. Coulson, *Nature* **1969**, 221, 1106.
- [19] C. A. Coulson, *Isr. J. Chem.* **1973**, 11, 683.
- [20] L. von Szentpály, *J. Phys. Chem. A* **2002**, 106, 11945.
- [21] J. E. Sansonetti and W. C. Martin, (Web Design) S. L. Young (2005), (*Electronic Handbook of Basic Atomic Spectroscopic Data* (version 1.1.2): <http://physics.nist.gov/Handbook>. National Institute of Standards and Technology, Gaithersburg, MD.
- [22] a) I. Eliezer, *Theor. Chim. Acta* **1970**, 18, 77; b) I. Eliezer, A. Reger, *Theor. Chim. Acta* **1972**, 26, 283.
- [23] M. Guido, G. Gigli, *J. Chem. Phys.* **1976**, 65, 1397.
- [24] K. J. Donald, W. H. Mulder, L. von Szentpály, *J. Chem. Phys.* **2003**, 119, 5423.
- [25] M. Hargittai, *Struct. Chem.* **2005**, 16, 33.
- [26] W. Kunciewicz-Kupczyk, J. Kapala, S. Roszak, M. Müller, *J. Chem. Phys.* **1998**, 108, 7743.
- [27] Incidentally, Kaupp and von Schnering (ref. [10 and 11]) obtained C_{2v} minimum-energy structures for the CdH_2 and HgH_2 dimers with the quasi-relativistic pseudopotential as well. For the ZnH_2 dimer, the D_{2h} structure was more stable.
- [28] W. Pies, A. Weiss in *Crystal Structure Data of Inorganic Compounds - Part a: Key Elements F, Cl, Br, I (VII Main Group) Halides and Complex Halides* (Eds.: K.-H. Hellwege, A. M. Hellwege), Landolt-Börnstein New Series III, vol. 7, Springer, Berlin: **1973**.
- [29] BeF_2 at ambient conditions is a three-dimensional extended solid with the β -cristabolite structure.
- [30] a) K. Burke, J. P. Perdew, Y. Wang, *Electronic Density Functional Theory: Recent Progress and New Directions* (Eds.: J. F. Dobson, G. Vignale, M. P. Das), Plenum Press, New York, **1998**; b) J. P. Perdew, K. Burke, Y. Wang, *Phys. Rev. B* **1996**, 54, 16533, and references therein.
- [31] a) D. E. Woon, T. H. Dunning, *J. Chem. Phys.* **1993**, 98, 1358; b) R. A. Kendall, T. H. Dunning, R. J. Harrison, *J. Chem. Phys.* **1992**, 96, 6796; c) T. H. Dunning, *J. Chem. Phys.* **1989**, 90, 1007.
- [32] H. Stoll, B. Metz, M. Dolg, *J. Comput. Chem.* **2002**, 23, 767.
- [33] K. A. Peterson, D. Figgen, E. Goll, H. Stoll, M. Dolg, *J. Chem. Phys.* **2003**, 119, 11113.
- [34] D. Figgen, G. Rauhut, M. Dolg, H. Stoll, *Chem. Phys.* **2005**, 227, 311.
- [35] K. A. Peterson, C. Puzzarini, *Theor. Chem. Acc.* **2005**, 114, 283.
- [36] See: D. Andrae, U. Häussermann, M. Dolg, H. Stoll, H. Preuss, *Theor. Chim. Acta* **1990**, 77, 123. Results from the (then newly introduced) MHF ECP and the optimized valence basis sets were described in this reference, but the parameters were not published in this work. The readers were asked to obtain details of the MHF ECPs and basis sets by writing to the authors. At present, the parameters for various elements are available at the web site of the Institute for Theoretical Chemistry of Stuttgart University: <http://www.theochem.uni-stuttgart.de/pseudopotentials/clickpse.html>.
- [37] Gaussian 03, Revision B.04, M. J. Frisch, et al. Gaussian, Inc., Pittsburgh PA, **2003**.
- [38] For comments on grid specification in Gaussian 03 see: *AE. Frisch, M. J. Frisch, G. W. Trucks, Gaussian 03 User's Reference*; Gaussian, Inc: Carnegie, PA, **2003**, pp. 121–122.
- [39] J. E. Carpenter, F. Weinhold, *J. Mol. Struct.* **1988**, 169, 41.
- [40] a) G. Kresse, J. Hafner, *Phys. Rev. B* **1993**, 47, 558; b) G. Kresse, Thesis, Technische Universität Wien, **1993**; c) G. Kresse, J. Furthmüller, *Comput. Mater. Sci.* **1996**, 6, 15; d) G. Kresse, J. Furthmüller, *Phys. Rev. B* **1996**, 54, 11169.
- [41] Density functional (energy minimization) calculations were performed by using the projector augmented wave (PAW) method within the generalized gradient approximation (GGA) as implemented in VASP. For each of the optimization runs a gamma centered grid was generated automatically, with the following subdivisions along the respective reciprocal lattice vectors specified manually: $15 \times 15 \times 15$ for the cubic fluorite (HgF_2); $6 \times 12 \times 14$ for the $HgCl_2$ (orthorhombic); $14 \times 12 \times 6$ for $HgBr_2$ (orthorhombic); and $14 \times 14 \times 6$ for the tetragonal red- HgI_2 structure. We accepted a 500 eV cutoff for the kinetic energies of the plane waves and an error (self consistent field tolerance) in the total energy of 1×10^{-5} eV per unit cell.
- [42] P. A. Akishin, V. P. Spiridonov, *Kristallografiya* **1957**, 2, 475. The error bars are understandably quite large in these early studies. In fact, linear geometries were determined in this study for all the Group 2 (alkaline earth) dihalides, as well. We now know (vide supra; see ref. [12], and references therein) that a number of them are unambiguously bent.
- [43] ED studies on ZnX_2 structures: a) M. Hargittai, J. Tremmel, I. Hargittai, *Inorg. Chem.* **1986**, 25, 3163. ($ZnCl_2$, $ZnBr_2$, and ZnI_2); b) G. V. Girichev, A. G. Gershikov, N. Yu. Subbotina, *Zh. Strukt. Khim.* **1988**, 29, 139; *Russ. J. Struct. Chem. (Engl. Transl.)* **1988**, 29, 945. (ZnF_2).
- [44] ED studies on CdX_2 structures: a) V. M. Petrov, A. N. Utkin, G. V. Girichev, A. A. Ivanov, *Zh. Strukt. Khim.* **1985**, 26, 52; *Russ. J. Struct. Chem. (Engl. Transl.)* **1985**, 26, 189 (A report on “three independent studies” on the structure of $CdBr_2$ using gas-phase electron diffraction GED); b) A. G. Gershikov, *Zh. Strukt. Khim.* **1989**, 30, 169; *Russ. J. Struct. Chem. (Engl. Transl.)* **1989**, 30, 841 ($CdBr_2$); c) A. Haaland, K.-G. Martinsen, J. Tremmel, *Acta Chem. Scand.* **1992**, 46, 589; d) N. Vogt, A. Haaland, K.-G. Martinsen, J. Vogt, *Acta Chem. Scand.* **1993**, 47, 937 ($CdCl_2$); e) N. Vogt, M. Hargittai, M. Kolonits, I. Hargittai, *Chem. Phys. Lett.* **1992**, 199, 441 (CdI_2).
- [45] ED studies on HgX_2 Structures: a) K. Kashiwabara, S. Konaka, M. Kimura, *Bull. Chem. Soc. Japan* **1973**, 46, 410 ($HgCl_2$); b) V. P. Spiridonov, A. G. Gershikov, B. S. Butayev, *J. Mol. Struct.* **1979**, 52, 53 (HgI_2); c) R. Z. Deyanov, K. P. Petrov, V. V. Ugarov, B. M. Shchedrin, N. G. Rambidi, *Zh. Strukt. Khim.* **1985**, 26, 58; *Russ. J. Struct. Chem. (Engl. Transl.)* **1985**, 26, 698 ($HgBr_2$).
- [46] a) J. W. Hastie, R. H. Hauge, J. L. Margrave, *High Temp. Sci.* **1969**, 1, 76. ZnF_2 was found to be bent with a wide error range of $154\text{--}170^\circ$; b) A. Givan, A. Loewenschuss, *J. Mol. Struct.* **1978**, 48, 325. In the series MX_2 ; $M = Zn, Cd$, and Hg ; $X = Cl, Br$, and I , all the Zn and Cd structures and HgI_2 were determined to be possibly linear, with large error ranges. However, $HgCl_2$ and $HgBr_2$ were determined to be nonlinear. See references in references [46a, and 47] for some of the earliest spectroscopic studies on the Group 12 dihalides.
- [47] a) A. Loewenschuss, A. Ron, O. Schnepf, *J. Chem. Phys.* **1968**, 49, 272; b) A. Loewenschuss, A. Ron, O. Schnepf, *J. Chem. Phys.* **1969**, 50, 2502.
- [48] Z. Varga, G. Lanza, C. Minichino, M. Hargittai, *Chem. Eur. J.* **2006**, 12, 8345.
- [49] M. L. Lesiecki, J. W. Nibler, *J. Chem. Phys.* **1976**, 64, 871.
- [50] P. Schwerdtfeger, P. D. W. Boyd, S. Brienne, J. S. McFeaters, M. Dolg, M.-S. Liao, W. H. E. Schwarz, *Inorg. Chim. Acta* **1993**, 213, 233.
- [51] a) M. Kaupp, M. Dolg, H. Stoll, H. G. von Schnering, *Inorg. Chem.* **1994**, 33, 2122; b) M. Kaupp, H. G. von Schnering, *Inorg. Chem.* **1994**, 33, 4179.
- [52] S. G. Wang, W. H. E. Schwarz, *J. Chem. Phys.* **1998**, 109, 7252.
- [53] M.-S. Liao, Q.-E. Zhang, W. H. E. Schwarz, *Inorg. Chem.* **1995**, 34, 5597.
- [54] a) N. B. Balabanov, K. A. Peterson, *J. Phys. Chem. A* **2003**, 107, 7465; b) N. B. Balabanov, K. A. Peterson, *J. Chem. Phys.* **2003**, 119, 12271; c) N. B. Balabanov, B. C. Shepler, K. A. Peterson, *J. Phys. Chem. A* **2005**, 109, 8765; d) B. C. Shepler, N. B. Balabanov, K. A.

- Peterson, *J. Phys. Chem. A* **2005**, *109*, 10363; e) B. C. Shepler, K. A. Peterson, *J. Phys. Chem. A* **2006**, *110*, 12321.
- [55] Mulliken (Absolute) electronegativities, $\chi_{(\text{Absolute})}$ from ref. [56] are used throughout this report. Indicative of similarities in the electron withdrawing power of Zn and Cd, $\chi_{(\text{Absolute})}$ for Zn (=4.45 eV) is somewhat larger than $\chi_{(\text{Absolute})}$ for Cd (=4.33 eV), while the Pauling electronegativity of Zn (=1.65) is slightly smaller than that of Cd (=1.69).
- [56] J. Emsley, *The Elements*, 3rd ed, Oxford University Press, New York, **1998**.
- [57] a) P. Pykkö, *Adv. Quantum Chem.*, **1978**, *11*, 353; for comments on the relativistic destabilization of the d atomic orbitals see Chapter XI. A.12. b) p. 566 of ref. [3].
- [58] P. P. Singh, *Phys. Rev. B* **1994**, *49*, 4954.
- [59] a) F. J. Keneshea, D. Cubicciotti, *J. Chem. Phys.* **1964**, *40*, 191; b) A. D. Bulanov, E. N. Verkhoturov, A. V. Makarov, A. N. Pronchatorov, *Vysokochist. Veshchestva* **1991**, *5*, 95.
- [60] K. Hilpert, L. Bencivenni, B. Saha, *J. Chem. Phys.* **1985**, *83*, 5227.
- [61] Geometrical parameters of these structures are given in Table S7 in the Supporting Information. For the CdCl₂ “Y-shaped” C_{2v}(1) dimer, the M–X contact between the two monomer fragments is exceptionally long (3.285 Å, which is ≈1.0 Å longer than the other M–X bonds in that structure). A similar elongation (≈0.9 Å) of the bridging M–X bond is observed in the analogous Hg₂F₄ C_{2v}(1) structure. For Zn₂F₄ C_{2v}(1) and Cd₂F₄ C_{2v}(1), the difference between the M–X bond is only about 0.5 Å.
- [62] These imaginary frequencies are for a pair of degenerate vibrations, which, if followed, each take us to a D_{2h} or C_{2h}(1) type structure with two terminal atoms, and two bridging halides.
- [63] It is curious that we obtain two imaginary frequencies ($n=2$) for the C_{3v} Zn₂Cl₄ structure (two degenerate distortions on the way apparently to the C_s and finally D_{2h} structure), and none for the other three C_{3v} Zn₂X₄ structures. However, the vibrational frequencies for the C_{3v} Zn₂Cl₄ structure (degenerate modes with $\nu=i14\text{ cm}^{-1}$) and the positive frequencies computed for the optimized Zn₂Br₄ and Zn₂I₄ geometries for the same degenerate vibrational modes ($\nu=5.3\text{ cm}^{-1}$ and $\nu=3.9\text{ cm}^{-1}$, respectively) are all very small. That the computed frequencies are imaginary for ZnCl₂ and real for Zn₂Br₄ and Zn₂I₄, may be due to subtle basis set effects; recall that the all electron cc-pVTZ basis set is used for the Cl sites while the MDF ECP and cc-pVTZ basis (for 25 outer electrons) are used for the Br and I sites.
- [64] J. B. Levy, M. Hargittai, *J. Phys. Chem. A* **2000**, *104*, 1950.
- [65] The trend in the bending of these linear MX₂ molecules is easy to understand considering that in all these molecules the M–X bond gets longer and weaker from the fluoride to the iodide (see Table 1 and S1 in the Supporting Information for the Group 12 and ref. [1] for the Group 2 dihalides).
- [66] To compute the dimerization energies, the counterpoise correction δ^{CP} , and $E^{\text{CP}}(\text{M}_2\text{X}_4)$, were obtained directly from our Gaussian 03 calculations. The definition of δ^{CP} and steps involved in calculating it are outlined in F. Jensen, *Introduction to Computational Chemistry*, Wiley, New York, **1999** pp. 172–173. $E^{\text{CP}}(\text{M}_2\text{X}_4)=E(\text{M}_2\text{X}_4)+\delta^{\text{CP}}$; and the computed counterpoise correction δ^{CP} is necessarily a positive value.
- [67] A. Schulz, M. Hargittai, *Chem. Eur. J.* **2001**, *7*, 3657.
- [68] P. Pykkö, F. Mendizabal *Inorg. Chem.* **1998**, *37*, 3018.
- [69] Note that for the similar C_{2h}-symmetry structure of the much less ionic but rather elusive Hg₂H₄, Pykkö suggested metallophilic attraction: P. Pykkö, M. Straka, *Phys. Chem. Chem. Phys.* **2000**, *2*, 2489.
- [70] C. Chieh, M. A. White, *Zeit. Krist.* **1984**, *166*, 189.
- [71] M. Hostetter, D. Schwarzenbach, *C. R. Chim.* **2004**, *8*, 147.
- [72] L. Pauling, *The Nature of the Chemical Bond*, Cornell University Press, Ithaca, NY, **1964**.
- [73] The availability of the filled 3d orbitals, and a larger separation between the 4s and 4p orbitals in Zn may help to account for some of the differences in the bonding patterns in the Mg and Zn dihalides. These include the relative instability of CdCl₂ structure of the ZnCl₂ and heavier dihalides, and the preference for a lower coordination (CN=4) at the Zn atom in those Zn dihalides.
- [74] *CRC Handbook of Chemistry and Physics*, 87th ed.; (Ed.: D. R. Lide), CRC Press, Boca Raton, FL, **2006–2007**.
- [75] The ionic radii used are those derived for the eight-coordinate M²⁺ ions. The values are from Section 12, pp. 11–12 of ref. [74]. The original references for the radii cited in ref. [74] are a) R. D. Shannon, *Acta Crystallogr. Sect. A* **1976**, *32*, 751; b) Y. Q. Jia, *J. Solid State Chem.* **1991**, *95*, 184.
- [76] See introduction section of ref. [11].
- [77] The ionic radii are those derived for the four- and six-coordinate M²⁺ ions. See ref. [72] and ref. [74], Section 12, pp. 11–12.
- [78] R. S. Nyholm, *Proc. Chem. Soc.* **1961**, 273.
- [79] L. E. Orgel, *J. Chem. Soc.* **1958**, 4186.
- [80] In ref. [71], Hostetter and Schwarzenbach argue for a 2 + 6 coordination at the Hg sites—corresponding to a distorted rhombohedron, rather than a distorted octahedron that would be the 2 + 4 coordination, as has been suggested earlier—see, for example, A. F. Wells, *Structural Inorganic Chemistry*, 3rd ed, Oxford, Clarendon Press, **1962**, p. 893.
- [81] Phase diagrams published in reference [71] span a range of roughly 400 K above room temperature and pressure up to about 6 GPa.
- [82] The Supporting Information contains Tables S1–S15; relativistic and non relativistic computational data obtained at the B3PW91 levels as described in detail in the methods section unless otherwise specified; Group 12 dihalide *Monomers*: Computed bending force constants, vibrational frequencies, computed (MP2) and experimental minimum energy geometries of the Group 12 dihalides and corresponding NBO orbital participation data; non-relativistic NBO charge, and orbital occupancy data; *Dimers*: relative energies of various possible dimer isomers and the corresponding numbers of imaginary frequencies; geometrical data for less competitive (C_{2v}(1), and C_{3v}) dimer structures; vibrational frequencies for the optimized D_{2h} and C_{2h} dimers, and the recomputed MP2 geometries; non-relativistic D_{2h} dimer geometries; stretching and bending contributions to the computed deformation energies. *Solids*: Melting points of the Groups 2 and 12 dihalides; Figure S1–S3 Computed bending potential energies for the Group 12 dihalides; Frontier Molecular Orbitals of the optimized ZnF₂, ZnI₂, HgF₂, and HgI₂. Unsigned (π -type) overlaps of frontier 2 π_g and 2 π_u MOs and the 1 π_u and 2 π_u MOs that are perpendicular to the plane of the model C_{2h}(1) type MX₂ dimer. The complete citation for reference [37].

Received: May 29, 2008

Revised: July 5, 2008

Published online: November 28, 2008